

Analyzing the competition of gamma rhythms with delayed pulse-coupled oscillators in phase representation

Atthaphon Viriyopase,^{1,2,3} Raoul-Martin Memmesheimer,^{1,3,4,5,6} and Stan Gielen^{1,2}

¹*Donders Institute for Brain, Cognition, and Behaviour, Radboud University Nijmegen, Nijmegen, The Netherlands*

²*Department of Biophysics, Faculty of Science, Radboud University Nijmegen, Nijmegen, The Netherlands*

³*Department of Neuroinformatics, Faculty of Science, Radboud University Nijmegen, Nijmegen, The Netherlands*

⁴*Center for Theoretical Neuroscience, Columbia University, New York, New York 10027, USA*

⁵*FIAS—Frankfurt Institute for Advanced Studies, Frankfurt am Main, Germany*

⁶*Neural Network Dynamics and Computation, Institute of Genetics, University of Bonn, Bonn, Germany*



(Received 3 July 2018; published 20 August 2018)

Networks of neurons can generate oscillatory activity as result of various types of coupling that lead to synchronization. A prominent type of oscillatory activity is gamma (30–80 Hz) rhythms, which may play an important role in neuronal information processing. Two mechanisms have mainly been proposed for their generation: (1) interneuron network gamma (ING) and (2) pyramidal-interneuron network gamma (PING). *In vitro* and *in vivo* experiments have shown that both mechanisms can exist in the same cortical circuits. This raises the questions: How do ING and PING interact when both can in principle occur? Are the network dynamics a superposition, or do ING and PING interact in a nonlinear way and if so, how? In this article, we first generalize the phase representation for nonlinear one-dimensional pulse coupled oscillators as introduced by Mirollo and Strogatz to type II oscillators whose phase response curve (PRC) has zero crossings. We then give a full theoretical analysis for the regular gamma-like oscillations of simple networks consisting of two neural oscillators, an “E neuron” mimicking a synchronized group of pyramidal cells, and an “I neuron” representing such a group of interneurons. Motivated by experimental findings, we choose the E neuron to have a type I PRC [leaky integrate-and-fire (LIF) neuron], while the I neuron has either a type I or type II PRC (LIF or “sine” neuron). The phase representation allows us to define in a simple manner scenarios of interaction between the two neurons, which are independent of the types and the details of the neuron models. The presence of delay in the couplings leads to an increased number of scenarios relevant for gamma-like oscillatory patterns. We analytically derive the set of such scenarios and describe their occurrence in terms of parameter values such as synaptic connectivity and drive to the E and I neurons. The networks can be tuned to oscillate in an ING or PING mode. We focus particularly on the transition region where both rhythms compete to govern the network dynamics and compare with oscillations in reduced networks, which can only generate either ING or PING. Our analytically derived oscillation frequency diagrams indicate that except for small coexistence regions, the networks generate ING if the oscillation frequency of the reduced ING network exceeds that of the reduced PING network, and vice versa. For networks with the LIF I neuron, the network oscillation frequency slightly exceeds the frequencies of corresponding reduced networks, while it lies between them for networks with the sine I neuron. In networks oscillating in ING (PING) mode, the oscillation frequency responds faster to changes in the drive to the I (E) neuron than to changes in the drive to the E (I) neuron. This finding suggests a method to analyze which mechanism governs an observed network oscillation. Notably, also when the network operates in ING mode, the E neuron can spike before the I neuron such that relative spike times of the pyramidal cells and the interneurons alone are not conclusive for distinguishing ING and PING.

DOI: [10.1103/PhysRevE.98.022217](https://doi.org/10.1103/PhysRevE.98.022217)

I. INTRODUCTION

Many processes in biology, physics, chemistry, and engineering have an oscillatory character. Regular oscillations on a limit cycle can be described by a single variable, the phase, which characterizes the time needed to reach the current state due to unperturbed dynamics when starting from some specified “reset” point on the cycle (e.g., [1,2]). If an oscillator receives inputs in the form of pulses and an input-induced perturbation from the limit cycle relaxes back sufficiently quickly (i.e., before the next input arrives), the system’s dynamics can be characterized by the phase together with a

function telling how the phase changes in response to an input pulse: the phase response curve (PRC) or the phase transition curve or transfer function [1,3,4]. This phase representation has been widely used to investigate network dynamics, especially synchronization and locking phenomena, in areas of science as diverse as neural circuits [5–8], technical networks [9,10], and insect behavior [4,11].

A particularly simple type of oscillator is given by a hybrid dynamical system whose state variable follows some one-dimensional, possibly nonlinear continuous dynamics, periodically reaches a threshold, and is then reset [12]. A rich source of such oscillators is the reduction of spiking neurons

to integrate-and-fire type neuron models [13–15]: Biological neurons possess a complicated branched structure with protrusions of different function and many slow and fast degrees of freedom associated with the resulting compartments. In integrate-and-fire type neuron models, this spatial structure is reduced to a single compartment “point neuron” and the high-dimensional dynamics are reduced to one degree of freedom, interpreted as the membrane potential [1,16]. Integrate-and-fire type neurons interact with pulses, mimicking spikes or action potentials; these are sent when the neuron is reset and are received by postsynaptic neurons often after some delay. In this article, we consider networks of two integrate-and-fire type neurons in phase representation to investigate the competition between mechanisms that are widely assumed to underlie oscillations in biological neural networks. Each integrate-and-fire type neuron thereby represents a synchronized population of neurons.

Oscillations in biological neural networks may be important for information processing [17,18]. One hypothesis is that they may coordinate precise spike sending of neurons and lead to synchronous spiking of neural populations [19]. Indeed, experiments have found examples of highly synchronous spiking associated with strong oscillations [20] and the timing of individual spikes relative to a global oscillation’s phase can carry important information [19,21–24]. Receiving neurons, in turn, can be highly sensitive to coincident input; in particular, types of synaptic plasticity depend on the timing of spikes [25]. Under high-input conditions the spike-generating mechanism can adaptively enhance the sensitivity to synchronous input while simultaneously decreasing the sensitivity to temporally uncorrelated inputs [26]. Further, oscillatory modulation of the membrane potential, for example, by input from a synchronously firing population of neurons, can provide a precise temporal window for the integration of synaptic inputs, favoring inputs arriving precisely at certain times [27,28]. The “communication through coherence” hypothesis suggests that this promotes information transmission between coherently oscillating neuron populations in different brain areas and allows us to focus on attended stimuli [29–32]. Higher frequency oscillations may support propagation and selection of information within areas [33,34]. Oscillation coordinated synchronous spiking across different neuron populations may also allow us to bind different features of a stimulus into a coherent percept [35–39] and generally parse and separate information into chunks of different length [22,40,41].

In the current article, we will focus on gamma (30–80 Hz) oscillations. These are prominent oscillations, which have been linked to input selectivity [30,42], spike-phase encoding [19,43], feature binding [35], as well as to storage and retrieval of information [40,41]. Mainly two mechanisms have been proposed to underlie gamma oscillations [44–46]. Both involve populations of excitatory pyramidal cells (E cells) and inhibitory interneurons (I cells). Tonic excitation of the interneurons, e.g., due to averaging slow excitatory input, can give rise to interneuron network gamma (ING) [47–52]: Imagine, by chance at some point more I cells spike and generate increased inhibition. This hinders the other I cells from spiking before the ones that have just spiked have recovered, and recruits them into synchrony such that a rhythm emerges [53]. The I cells undergo a cycle of enhanced spiking

activity, resulting in increased recurrent inhibition within the population, subsequently decreased activity, followed by recovery from inhibition and again enhanced spiking. The resulting periodically increased inhibition generates rhythmic spiking in connected E cells. Pyramidal-interneuron network gamma (PING) is mediated by interacting populations of E cells and I cells [51,54,55]. Imagine, by chance at some point more E cells spike. The I cells respond to the increased excitatory input from the E cells by increasing their spiking. The resulting increased inhibitory input in turn hinders spiking in the E cells, such that their activity goes down. The lack of excitatory input leads to a decrease of I-cell activity, such that the E cells can recover from inhibition and generate increased spiking, which completes the cycle. To summarize, ING relies crucially on mutual inhibition generated by the I cells among each other, while PING relies crucially on the $E \rightarrow I$ connections and the inhibitory feedback to the E cells. In model networks, there can be a sharp boundary in parameter space between the regime in which the I cells have weak enough drive for PING, and the ING regime in which the drive to the I cells is so large that they fire without being prompted by the E cells [56]. However, recent studies have shown that this sharp transition may be a simplification [57] and we highlighted in Ref. [58] that there are two-neuron systems that can generate ING as well as PING, depending on the initial conditions.

Using computer simulations of larger networks, in Ref. [58] we have shown that in the range of parameter space where ING and PING may in principle be expected to exist, both mechanisms compete such that the mechanism generating the higher oscillation frequency “wins”; i.e., the mechanism with the higher frequency determines the frequency of the network oscillation and suppresses the other one. In the current article we provide a theoretical analysis of the finding, using simplified networks of two oscillating integrate-and-fire type neurons. The simplified system allows us to analytically study the interactions between ING and PING and to better understand their consequences for oscillations in networks of interacting E cells and I cells. The analytically tractable model consists of an E neuron, which belongs to the category of type I neurons, and an I neuron, which can be either type I or type II. For type I neurons an excitatory input always advances the next spike; the PRC is entirely positive. In contrast, an excitatory input arriving at a type II neuron can also delay the next spike; the PRC is partially negative [1,59]. Indeed, there is experimental evidence that I cells involved in gamma oscillations may belong to the category of type II neurons [60–62].

We consider current-based integrate-and-fire neurons, where the currents have infinitesimally short temporal duration. The latter implies that the membrane potential responds in jumplike manner to the input, the former that the height of the jump is independent of the membrane potential. Note that also some conductance-based and more general models can be cast into this form by a transformation of variables [63,64]. For type I neurons, where an excitatory jump (towards the membrane potential threshold) always advances the phase, a phase representation has been derived in Refs. [4,65]. We adopt this phase representation for our type I neurons since the linearization of the free dynamics strongly simplifies the analytical study of the system and since the phase representation allows for

simple and fast event-based numerical simulations. To be able to study networks with type II interneurons in the same way, we derive a generalized phase representation, which is applicable to neurons of this type. For this, we assume that an infinitesimal phase response curve (iPRC) of type II is given, and we derive the corresponding membrane potential dynamics as well as the PRC.

The article is structured as follows: Section II is dedicated to the standard phase representation of a one-dimensional oscillator, its derivation from the free dynamics, and its application to the leaky integrate-and-fire (LIF) neuron, which is the type I neuron model that we use throughout the article. In Sec. III, we derive the phase representation of one-dimensional oscillators of type II, where the iPRC can change sign. We apply the scheme to derive the “sine neuron,” the type II neuron model that we use throughout the article. The Appendix compares this neuron with the radial isochron clock, an oscillator model that has the same iPRC. In Sec. IV, we consider delayed pulse-coupled networks of two model neurons and show the ways in which they interact depending on their phase difference. This yields a representation of the dynamics in terms of iteration maps whose fixed points yield the regular oscillations that we study in Sec. V. Section VI is dedicated to the competition and coexistence of the ING and PING oscillation mechanisms. We conclude with a discussion in Sec. VII, which puts our findings in context to the existing literature and our previous larger scale simulation studies [58]. We note that in Ref. [58] we summarized, displayed, and discussed some of the results of the current article.

II. PHASE REPRESENTATION OF TYPE I ONE-DIMENSIONAL OSCILLATORS

A. General theory

In the following, we review the standard phase representation of one-dimensional oscillators coupled by infinitesimally short pulsed interactions proposed in Refs. [4,8,65], as needed for the purposes of the present article. For a more general derivation and discussion, see [65].

A one-dimensional neural oscillator is generally characterized by a voltage-like state variable V . We assume that without arrival of fast inputs, V is strictly increasing up to a spike threshold $\Theta_V > 0$. When reaching the threshold at a time t , $V(t) = \Theta_V$, V is reset to zero, i.e., $V(t^+) = 0$, and starts increasing again. We denote the period of these free dynamics by T . We note that when $V(t)$ is specified by an autonomous differential equation (the function specifying the rate of change of V does not depend on time) with unique solutions, trajectories cannot cross or overlap and furthermore the oscillatory behavior forbids fixed points. This implies strict monotonicity of V except where V is being reset.

We now introduce a so-called phase variable $\varphi(t)$, which increases with slope one in absence of fast input,

$$\frac{d\varphi(t)}{dt} = 1, \quad (1)$$

and has a phase threshold Θ . When φ reaches the threshold at a time t , $\varphi(t) = \Theta$, the phase is reset to zero, $\varphi(t^+) = 0$. Note that Eq. (1) implies that the free period of the phase is Θ . Since we want to map $\varphi(t)$ to $V(t)$, we choose the free

periods identical, $\Theta = T$. The strict monotonicity of $V(t)$ then implies that there is a strictly monotonic, bijective so-called rise function U , mapping phase φ to voltage V , i.e., at time t

$$V(t) = U(\varphi(t)). \quad (2)$$

In particular, Θ_V and Θ are related by

$$\Theta_V = U(\Theta). \quad (3)$$

For the LIF neuron, the type I neuron we focus on in our study, $U:]-\infty, \Theta] \rightarrow]-\infty, \Theta_V]$ (depending on the neuron model domain and/or codomain are different). U can be derived directly from free membrane potential dynamics: Consider free membrane potential dynamics \tilde{V} , which start at the reset potential at $t = 0$, i.e., $\tilde{V}(0) = 0$. \tilde{V} can be continued for negative times towards $-\infty$ (or a possible lower bound) and for positive times to Θ_V . The analogous dynamics of φ run from $-\infty$ (or a possible lower bound) to $\Theta = T$ with $\varphi(0) = 0$. We have $U(\varphi) = \tilde{V}(\varphi)$, since time equals phase for the considered piece of dynamics.

When φ reaches the phase threshold, it is reset and a spike is emitted. After a delay time τ , the spike arrives at postsynaptic neurons at, say, time t_a . We assume that they respond with an instantaneous jump in their membrane potential. The strength ε of the coupling from the pre- to the postsynaptic neuron specifies the height of the jump. The corresponding phase jump is computed using a transfer function H ,

$$\varphi(t_a^+) = H(\varphi(t_a), \varepsilon). \quad (4)$$

For convenience, we will omit t_a and use φ instead of $\varphi(t_a)$. If an input of strength ε is subthreshold, i.e., $U(\varphi) + \varepsilon < \Theta_V$, the transfer function is given by

$$H(\varphi, \varepsilon) = U^{-1}(U(\varphi) + \varepsilon). \quad (5)$$

We may understand this formula as follows: We take φ and change to the membrane potential domain using U given in Eq. (2). We know that in the membrane potential domain an input of strength ε additively changes the membrane potential $U(\varphi)$ by ε . We compute the corresponding phase, i.e., the phase after the input, using U^{-1} . The composition of the steps, $U^{-1}(U(\varphi) + \varepsilon)$, maps the phase before the interaction to the phase after the interaction. We note that $H(\varphi, \varepsilon)$ is strictly monotonically increasing, both as a function of ε and of φ , since U and thus U^{-1} are strictly monotonically increasing. Since suprathreshold input leads to immediate spiking and reset of the neuron, we need to extend the definition of the transfer function to

$$H(\varphi, \varepsilon) = U^{-1}(U(\varphi) + \varepsilon), \quad \text{for } U(\varphi) + \varepsilon < \Theta_V, \quad (6)$$

$$H(\varphi, \varepsilon) = 0, \quad \text{for } U(\varphi) + \varepsilon \geq \Theta_V. \quad (7)$$

$H(\varphi, \varepsilon)$ yields the new phase of a neuron when it receives an input ε at phase φ [cf. Eq. (4)]. It is thus closely related to the PRC $P(\varphi, \varepsilon)$ (e.g., [3]), which yields the phase change induced by an input ε received at phase φ ,

$$P(\varphi, \varepsilon) = H(\varphi, \varepsilon) - \varphi. \quad (8)$$

The iPRC $Z(\varphi)$ characterizes the phase shift of a neuron around $\varepsilon = 0$; i.e., an infinitesimal input $d\varepsilon$ generates an infinitesimal

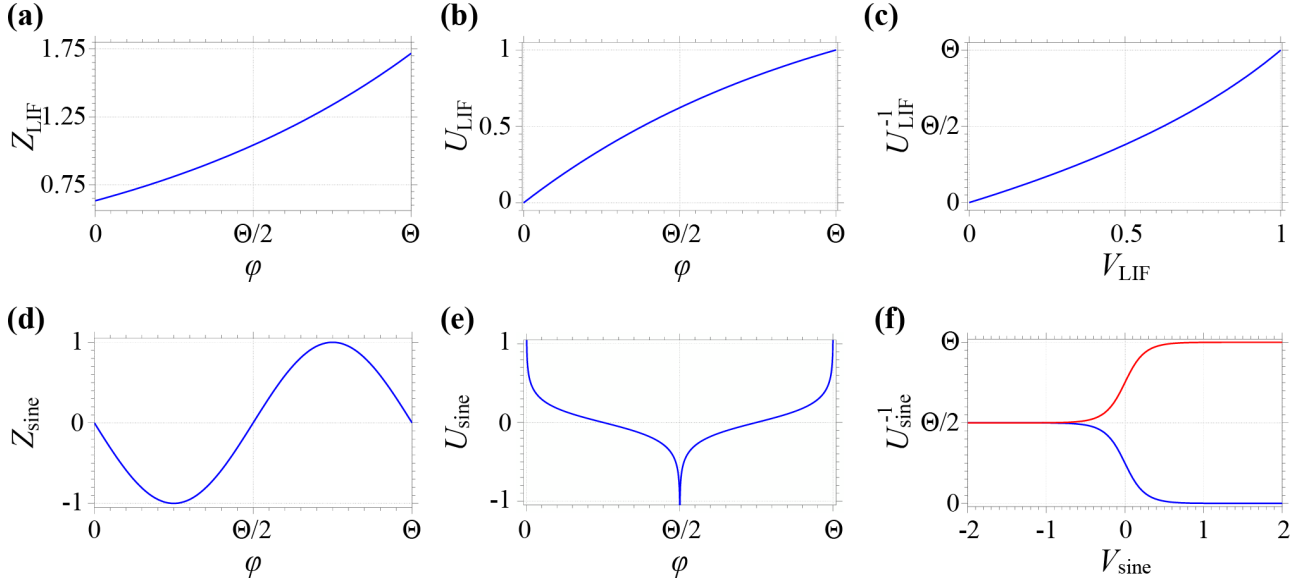


FIG. 1. Infinitesimal phase response curves (iPRC) Z , rise functions (U), and inverse rise functions (U^{-1}) for the type I leaky integrate-and-fire neuron and the type II sine neuron. Upper panels show (a) the iPRC, (b) the rise function, and (c) the inverse rise function for the leaky integrate-and-fire neuron. Corresponding data are shown in the lower panels (d), (e), and (f) for the sine neuron; its inverse rise function has two branches (blue: $k = 1$, red: $k = 2$). Parameter setting: $\gamma = 1$, $\Theta_V = 1$, and $\Theta = 1$.

phase shift

$$d\varphi = Z(\varphi)d\varepsilon. \quad (9)$$

For small ε around 0 we have $P(\varphi, \varepsilon) \approx Z(\varphi)\varepsilon$; $H(\varphi, \varepsilon) \approx \varphi + Z(\varphi)\varepsilon$. $Z(\varphi)$ and $H(\varphi, \varepsilon)$ are thus related by

$$Z(\varphi) = \left. \frac{\partial H(\varphi, \varepsilon)}{\partial \varepsilon} \right|_{\varepsilon=0}. \quad (10)$$

As mentioned above, U^{-1} is strictly increasing. Equations (6) and (8) then imply that H and P are strictly increasing in ε for subthreshold input. Because $P(\varphi, 0)$ equals 0, $P(\varphi, \varepsilon) > 0$ for $\varepsilon > 0$ and subthreshold input. In other words, the PRC has to be of type I; the formalism is thus applicable to type I neurons only.

B. The LIF neuron in phase representation

We now review the derivation of the phase representation for the type I LIF neuron using the methods described in Sec. II A (cf. also [65]). The dynamics of the membrane potential $V_{\text{LIF}}(t)$ of the LIF neuron are given by

$$\frac{dV_{\text{LIF}}(t)}{dt} = -\gamma V_{\text{LIF}}(t) + I, \quad (11)$$

where γ represents the inverse of the membrane time constant and I captures the external driving current. When the membrane potential reaches its threshold Θ_V , the neuron spikes and the membrane potential is reset to zero. A spike

arriving at time t at a synaptic connection with strength ε induces an instantaneous change in the membrane potential, i.e., $V_{\text{LIF}}(t^+) = V_{\text{LIF}}(t) + \varepsilon$. We assume that slow external inputs add up to a constant current I , which drives the neuron continuously over the threshold, such that it oscillates ‘‘intrinsically’’ in absence of fast synaptic input. This allows us to define the phase $-\infty < \varphi \leq \Theta$, which increases with slope 1 and is reset to zero when it reaches Θ , where also a spike is emitted.

The rise function U linking the phase φ of the spiking cycle to the membrane potential description V can be determined as described in Sec. II A as

$$V_{\text{LIF}} = U_{\text{LIF}}(\varphi) = \frac{I}{\gamma}(1 - e^{-\gamma\varphi}) \quad (12)$$

(see [4,65]), yielding the inverse

$$U_{\text{LIF}}^{-1}(V_{\text{LIF}}) = \frac{1}{\gamma} \ln \left(\frac{I}{I - \gamma V_{\text{LIF}}} \right). \quad (13)$$

U_{LIF} is a monotonically increasing function of φ . Figures 1(b) and 1(c) show the rise function U_{LIF} and its inverse U_{LIF}^{-1} , respectively. The phase threshold is explicitly given in terms of the voltage threshold Θ_V by

$$\Theta = U_{\text{LIF}}^{-1}(\Theta_V) = \frac{1}{\gamma} \ln \left(\frac{I}{I - \gamma \Theta_V} \right). \quad (14)$$

U_{LIF} and U_{LIF}^{-1} yield the transfer function of the LIF neuron

$$H_{\text{LIF}}(\varphi, \varepsilon; \Theta_V) = \begin{cases} -\frac{1}{\gamma} \ln \left(e^{-\gamma\varphi} - \frac{\gamma\varepsilon}{I} \right), & \text{for } U_{\text{LIF}}(\varphi) + \varepsilon < \Theta_V, \\ 0, & \text{for } U_{\text{LIF}}(\varphi) + \varepsilon \geq \Theta_V; \end{cases} \quad (15)$$

$$0, \quad \text{for } U_{\text{LIF}}(\varphi) + \varepsilon \geq \Theta_V; \quad (16)$$

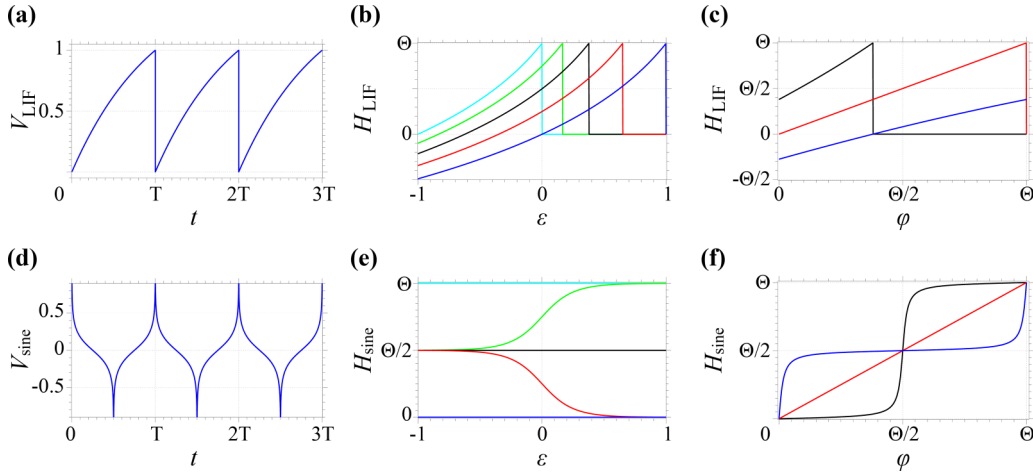


FIG. 2. Free dynamics (V) and transfer functions (H) for the type I leaky integrate-and-fire neuron and the type II sine neuron. Upper panels show (a) the free membrane potential dynamics, (b) the transfer function as a function of the coupling strength ε for different constant values of the phase φ at input arrival (blue, red, black, green, cyan: $\varphi = 0, 0.25, 0.5, 0.75,$ and 1), and (c) the transfer function as a function of φ for different constant ε (blue, red, black: $\varepsilon = -0.5, 0,$ and 0.5) for the LIF neuron. Lower panels (d)–(f) show the corresponding plots for the sine neuron. Parameter setting: $\gamma = 1$, $\Theta_V = 1$, and $\Theta = 1$.

cf. Eqs. (6) and (7). It is displayed in Fig. 2, panels (b) and (c).

Note that the phase φ can assume all values within $]-\infty, \Theta]$, where negative phases are generated by inhibitory inputs that cause hyperpolarization of the membrane potential. Since we use the convention that the phase φ is reset to zero when it reaches the threshold Θ , at the time of a spiking due to the driving current we have $\varphi = \Theta$ rather than $\varphi = 0$. Since $\gamma > 0$, we can set $\gamma = 1$ and $\Theta_V = 1$ after appropriate scaling of time and voltage, without loss of generality for a single neuron. For simplicity, we assume that in networks with two type I neurons the membrane time constants are the same, such that the scaling is possible. The driving current I

that gives $U_{\text{LIF}}(\Theta) = 1$ follows in a straightforward way from Eq. (12),

$$I = \frac{1}{1 - e^{-\Theta}}. \quad (17)$$

The rise function Eq. (12) and its inverse Eq. (13) are then given by

$$U_{\text{LIF}}(\varphi) = \frac{1 - e^{-\varphi}}{1 - e^{-\Theta}}, \quad (18)$$

$$U_{\text{LIF}}^{-1}(V_{\text{LIF}}) = -\ln[1 - (1 - e^{-\Theta})V_{\text{LIF}}]. \quad (19)$$

Equations (15) and (16) yield the transfer function

$$H_{\text{LIF}}(\varphi, \varepsilon; \Theta) = \begin{cases} -\ln[e^{-\varphi} - (1 - e^{-\Theta})\varepsilon], & \text{for } U_{\text{LIF}}(\varphi) + \varepsilon < 1, \\ 0, & \text{for } U_{\text{LIF}}(\varphi) + \varepsilon \geq 1, \end{cases} \quad (20)$$

and, according to Eq. (10), the iPRC is given by

$$Z_{\text{LIF}}(\varphi; \Theta) = (1 - e^{-\Theta})e^{\varphi}, \quad (22)$$

which is shown in Fig. 1(a).

III. PHASE REPRESENTATION OF TYPE II ONE-DIMENSIONAL OSCILLATORS

A. General theory

The phase representation Sec. II is only valid for one-dimensional neurons of type I, such as the LIF neuron. In the following we generalize it to neurons of type II, whose iPRC has negative and positive parts. We assume that our type II neuron is a current-based one-dimensional oscillator, which receives current inputs of infinitesimally small temporal extent. These generate jumplike responses in the membrane potential; the height of the jump is independent of the voltage. We further assume that the membrane dynamics are at first

unknown, and the neuron dynamics are instead specified by an infinitesimal phase response curve, which specifies the phase response to input pulses of infinitesimally small strength. We then derive the free membrane dynamics as well as the full phase representation. They turn out to follow nearly uniquely from the iPRC for the considered class of oscillator models.

The domain of the iPRC can be divided into several intervals, in which the iPRC has the same sign (positive or negative). As an example, for a type I iPRC that is everywhere larger than zero, we have only one interval $]-\infty, \Theta[$; cf. the LIF neuron in Sec. II B. For a sine-like type II iPRC, cf. Sec. III B below, there are two subintervals $]0, \Theta/2[$, $]\Theta/2, \Theta[$, and the iPRC becomes zero at the ends of the intervals. We aim to construct rise functions for each subinterval and combine them to obtain the transfer function H .

Restricted to a single interval i , the iPRC is either completely positive or negative. A strictly increasing free voltage implies a positive iPRC: A small upward jump in the voltage

maps the current state to a state that would be reached in the future by free evolution; cf. Sec. II. A strictly decreasing free voltage implies a negative iPRC, as an upward jump in the voltage maps the current state to an earlier state. In turn, a positive (negative) iPRC implies monotonically increasing (decreasing) free voltage dynamics. We note that this implies that a differential equation specifying V must switch between intervals with different signs of the iPRC (cf. Sec. III B below). In interval i we can define a monotonically increasing or decreasing transfer function U_i , which maps phase to voltage, cf. Eq. (2), as follows: For given φ , there are sufficiently small inputs ε such that the voltage and phase stay within the interval even if i is the interval neighboring the threshold. Then, the transfer function is given by Eq. (5) and

$$\frac{\partial H_i(\varphi, \varepsilon)}{\partial \varepsilon} = \frac{1}{U_i'(U_i^{-1}(U_i(\varphi) + \varepsilon))}. \quad (23)$$

By setting ε to 0, see Eq. (10), we obtain for all φ in the interval

$$Z(\varphi) = \left. \frac{\partial H_i(\varphi, \varepsilon)}{\partial \varepsilon} \right|_{\varepsilon=0} = \frac{1}{U_i'(U_i^{-1}(U_i(\varphi)))} = \frac{1}{U_i'(\varphi)}. \quad (24)$$

The slope of $U_i(\varphi)$ specifies $U_i(\varphi)$ up to a constant, so $U_i(\varphi)$ is basically the antiderivative $F_i(\varphi)$ of $1/Z(\varphi)$ in interval i ,

$$F_i(\varphi) = \int \frac{1}{Z(\varphi)} d\varphi. \quad (25)$$

We obtain $U_i(\varphi)$ from $F_i(\varphi)$ by specifying the voltage at some phase.

When φ approaches an interval boundary where the iPRC has a zero, $U_i(\varphi)$ and thus the voltage will usually tend to $\pm\infty$, which we then take as the value assumed by the rise function there. We note that the voltage can tend to $+\infty$ even if the phase is not in the interval neighboring the threshold. Then the phase does not reach the phase threshold and the neuron does not spike. Models with this property may be interpreted as having a history-dependent voltage spike threshold. We note that our formalism allows us to construct oscillator models from the iPRC for which $U_i(\varphi)$ does not have a reasonable biological interpretation in terms of a voltage. As an example, an iPRC that is negative in the interval adjacent to the phase threshold can give rise to a $U_i(\varphi)$ that reaches $-\infty$ as the phase approaches the phase threshold and the neuron spikes.

If ε does not lead the dynamics out of interval i , the transfer function is given by

$$H_i(\varphi, \varepsilon) = U_i^{-1}(U_i(\varphi) + \varepsilon). \quad (26)$$

It is uniquely determined by the iPRC, since adding a constant to U_i , i.e., using $U_{i,c_i}(\varphi) = U_i(\varphi) + c_i$ to define H_i , does not change it,

$$\begin{aligned} H_i(\varphi, \varepsilon) &= U_{i,c_i}^{-1}(U_{i,c_i}(\varphi) + \varepsilon) = U_i^{-1}(U_i(\varphi) + c_i + \varepsilon - c_i) \\ &= U_i^{-1}(U_i(\varphi) + \varepsilon). \end{aligned} \quad (27)$$

We can derive the rise function also in a more intuitive manner as follows: An input to our neuron models should have the same effect whether we apply it at once or in small pieces, which we may imagine to be separated by small temporal

differences. Indeed, in the membrane potential representation, the input is simply additive, so this is certainly satisfied. In phase representation, it should be satisfied as well. An input $d\tilde{\varepsilon}$ arriving at phase φ leads in linear approximation to a new phase $\varphi^+ = \varphi + Z(\varphi)d\tilde{\varepsilon}$. If the change due to an input piece $d\tilde{\varepsilon}$ does not depend on the total input ε , we should get the same change, if the previous phase has been reached due to a previous piece $\tilde{\varepsilon}$ of an input. Denoting the phase before the arrival of $d\tilde{\varepsilon}$ by $\varphi(\tilde{\varepsilon})$, we find that the input $\tilde{\varepsilon} + d\tilde{\varepsilon}$ leads to the phase $\varphi(\tilde{\varepsilon} + d\tilde{\varepsilon}) = \varphi(\tilde{\varepsilon}) + Z(\varphi(\tilde{\varepsilon}))d\tilde{\varepsilon}$. Note that $\varphi(\tilde{\varepsilon})$ is the exact nonapproximated phase after receiving $\tilde{\varepsilon}$, while the impact of $d\tilde{\varepsilon}$ is covered up to first order. Knowing the impact of an additional input $d\tilde{\varepsilon}$ up to first order (equivalently, the impact of an infinitesimal input) allows us to write the phase change in the form of a differential equation,

$$\frac{d\varphi(\tilde{\varepsilon})}{d\tilde{\varepsilon}} = Z(\varphi(\tilde{\varepsilon})). \quad (28)$$

Since the impact of an input piece does not explicitly depend on the previously received input, the right-hand side does not explicitly depend on the independent variable $\tilde{\varepsilon}$, but only via $\varphi(\tilde{\varepsilon})$. In other words, the phase change $\varphi(\tilde{\varepsilon})$ is characterized by an autonomous ordinary differential equation. In the Appendix, we highlight that general phase oscillators do not have this property, using the radial isochron clock. Note that Eq. (28) can also be derived by discretizing the timelike variable ε into many small steps of size $d\tilde{\varepsilon}$, expanding the PRC around zero coupling strength by its Taylor series, and taking the limit of $d\tilde{\varepsilon} \rightarrow 0$.

Solving Eq. (28) by separation of variables, we obtain

$$\int_{\varphi}^{\varphi^+} \frac{1}{Z(\varphi)} d\varphi = \int_0^{\varepsilon} d\tilde{\varepsilon} = \varepsilon, \quad (29)$$

where φ^+ and φ are the phases before and after arrival of the total subthreshold input ε . By the first fundamental theorem of calculus, we have $F_i(\varphi^+) - F_i(\varphi) = \varepsilon$, where again $F_i(\varphi) = \int 1/Z(\varphi)d\varphi$. Since on the other hand

$$U_i(\varphi^+) - U_i(\varphi) = \varepsilon, \quad (30)$$

F_i equals U_i up to an additive constant and U_i is basically the antiderivative of $1/Z(\varphi)$ in the interval i .

Equation (28) and its property of being autonomous can also be directly derived from the fact that dV_i (the change of the voltage due to $d\tilde{\varepsilon}$) does not explicitly (not even implicitly) depend on already applied subthreshold input: While receiving an input, V_i may be seen as a function $V_i(\tilde{\varepsilon})$ of the already applied piece of input $\tilde{\varepsilon}$, with initial value $V_i(0) = V_i$ and $\tilde{\varepsilon}$ running from 0 to ε . $V_i(\tilde{\varepsilon})$ then satisfies the autonomous differential equation $dV_i(\tilde{\varepsilon})/d\tilde{\varepsilon} = 1$. This implies $dU_i(\varphi(\tilde{\varepsilon}))/d\tilde{\varepsilon} = 1$ and, after application of the chain rule, the differential equation $d\varphi(\tilde{\varepsilon})/d\tilde{\varepsilon} = 1/U_i'(\varphi(\tilde{\varepsilon}))$. Since for $\tilde{\varepsilon} = 0$ the left-hand side equals $Z(\varphi)$ and the differential equation is autonomous, we have $1/U_i'(\varphi) = Z(\varphi)$ for all phases. This implies that $\varphi(\tilde{\varepsilon})$ satisfies Eq. (28) and it implies Eq. (30).

Equation (28) also allows us to directly derive the transfer function and thus the complete phase representation from the iPRC. We note that $\varphi(\tilde{\varepsilon}) = H_i(\varphi, \tilde{\varepsilon})$ and rewrite Eq. (28) as

$$\frac{\partial H_i(\varphi, \tilde{\varepsilon})}{\partial \tilde{\varepsilon}} = Z(H_i(\varphi, \tilde{\varepsilon})) \quad (31)$$

with initial condition $H_i(\varphi, 0) = \varphi$, which reduces to Eq. (10) for $\tilde{\varepsilon} = 0$. Solving the differential equation yields the transfer function in interval i .

Phases φ where the iPRC is zero are fixed points of the dynamics Eqs. (28) and (31). Thus, under weak conditions on Eq. (28) (the iPRC is globally Lipschitz continuous such that the differential equation has a unique solution existing for all ε), such a φ will not be changed by input, $H_i(\varphi, \varepsilon) = \varphi = \text{constant}$; furthermore, no finite input will lead beyond the borders of an interval i where the iPRC gets zero.

B. The sine neuron in phase representation

Typical type II neurons show a phase delay in response to excitatory input $\varepsilon > 0$ arriving at small phases (early in the spiking cycle, shortly after a spike) and a phase advance when such input arrives at larger phases [3,57]. With these characteristics in mind, we define our type II neurons as “sine neurons” by an iPRC,

$$Z_{\text{sine}}(\varphi) = -\sin\left(\frac{2\pi}{\Theta}\varphi\right), \quad (32)$$

where $\varphi \in [0, \Theta]$ [see Fig. 1(d)] and $\Theta \equiv T$ is the period and the phase threshold of the neuron. We use the sinusoidal function as the iPRC of our type II neurons also because neuron models such as the Hodgkin-Huxley neuron can undergo Hopf bifurcations [66,67] and the normal form oscillator of Hopf bifurcating systems and thus general Hopf bifurcating systems with appropriate parameters have near the bifurcation for suitable inputs a sinusoidal iPRC Eq. (32) [68]. To facilitate the analytical study of two-neuron networks that include type II neurons, we apply the phase oscillator formalism to the sine neuron. Since the iPRC changes sign, we use the methodology derived in Sec. III A.

We split the interval domain $[0, \Theta]$ of Z_{sine} into two, i.e., $]0, \Theta/2[$ and $]\Theta/2, \Theta[$, and treat $U_{\text{sine}}(\varphi)$ at $\varphi \in \{0, \Theta/2, \Theta\}$ separately. Equations (25) and (32) yield the rise functions for the first subinterval ($U_{\text{sine},1}(\varphi)$, $\varphi \in]0, \Theta/2[$) and for the second subinterval ($U_{\text{sine},2}(\varphi)$, $\varphi \in]\Theta/2, \Theta[$): $U_{\text{sine},k}(\varphi) = -\Theta \ln[|\tan(\pi\varphi/\Theta)|]/2\pi + c_k$, where $c_k \in \mathbb{R}$ and $k \in \{1, 2\}$. From the first subinterval, we compute the values of the rise function at $\varphi = 0$ and $\varphi = \Theta/2$, $U_{\text{sine}}(0) = \lim_{\varphi \rightarrow 0^+} U_{\text{sine},1}(\varphi) = \infty$, $U_{\text{sine}}(\Theta/2) = \lim_{\varphi \rightarrow \Theta/2^-} U_{\text{sine},1}(\varphi) = -\infty$. Compatible with this, $\lim_{\varphi \rightarrow \Theta/2^+} U_{\text{sine},2}(\varphi) = -\infty$. Finally, at $\varphi = \Theta$, $U_{\text{sine}}(\Theta) = \lim_{\varphi \rightarrow \Theta^-} U_{\text{sine},2}(\varphi) = \infty$. In summary, the rise function of the sine neuron is given by

$$U_{\text{sine}}(\varphi) = \begin{cases} \infty, & \text{for } \varphi \in \{0, \Theta\}, \\ -\infty, & \text{for } \varphi = \Theta/2, \\ -\frac{\Theta}{2\pi} \ln \left[\tan\left(\frac{\pi}{\Theta}\varphi\right) \right] + c_1, & \text{for } \varphi \in]0, \frac{\Theta}{2}[, \\ -\frac{\Theta}{2\pi} \ln \left[\tan\left(-\frac{\pi}{\Theta}\varphi\right) \right] + c_2, & \text{for } \varphi \in]\frac{\Theta}{2}, \Theta[. \end{cases} \quad (33)$$

Figure 1(e) illustrates the rise function $U_{\text{sine}}(\varphi)$ for the sine neuron with $c_1 = c_2 = 0$.

Since the membrane potential of our sine neuron satisfies $V_{\text{sine}}(t) = U_{\text{sine}}(\varphi(t))$, it reaches $+\infty$ in finite time [see Fig. 1(e)]. We can thus set the spike threshold to ∞ . In this respect, the sine neuron resembles the theta or quadratic

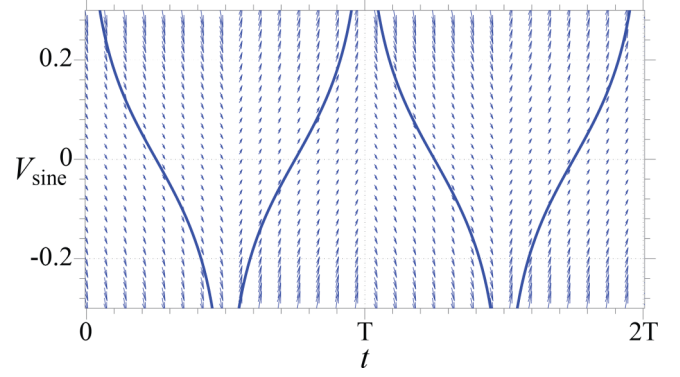


FIG. 3. Vector field of the sine neuron defined by Eqs. (34) and (35). The solid curves represent $V_{\text{sine}}(t) = U_{\text{sine}}(\varphi(t))$ for $c_1 = c_2 = 0$. The vector field switches when V_{sine} reaches $+\infty$ or $-\infty$.

integrate-and-fire model (see, e.g., [1] and Sec. VII). However, the sine neuron is not reset to $-\infty$. When it reaches threshold, the membrane potential decreases from $+\infty$ to $-\infty$ halfway through the cycle by its intrinsic dynamics. In this regime, excitatory input yields a phase delay. Thereafter the membrane potential increases gradually to $+\infty$ in a regime where excitation yields a phase advance. The dynamical regime thus depends on the last “event.” If the last event was sending a spike ($V_{\text{sine}} = \infty$), we are in regime $k = 1$, where excitation delays the phase. If the last event was reaching the reset potential ($V_{\text{sine}} = -\infty$), we are in regime $k = 2$, where excitation advances the phase. Note that this is an extension to the dynamics of standard integrate-and-fire models, where neurons are only in one dynamical regime and reset in an infinitesimally short time after they reach threshold. In contrast to the “spike response” extension (see [69]), the dynamical regime in our extension does not only depend on the time elapsed since spike sending, but also on the full dynamics of the neuron. A stronger asymmetry between spiking and reset or a more rapid onset of spikes can be easily achieved by modifying the sinusoidal shape of the iPRC.

Interestingly, the membrane potential of our sine neuron obeys the simple nonlinear differential equation

$$\frac{dV_{\text{sine}}(t)}{dt} = \frac{dU_{\text{sine}}(\varphi)}{d\varphi} \frac{d\varphi(t)}{dt} = -\cosh\left[\frac{2\pi}{\Theta}V_{\text{sine}}(t)\right] \quad (34)$$

in the regime $k = 1$, i.e., if the previous event was a spike, and it obeys

$$\frac{dV_{\text{sine}}(t)}{dt} = \cosh\left[\frac{2\pi}{\Theta}V_{\text{sine}}(t)\right] \quad (35)$$

in the regime $k = 2$, i.e., if the previous event was a reset; cf. Fig. 3.

Using Eq. (33), we can define an inverse function U_{sine}^{-1} with two branches; see Fig. 1(f). For the branch $k = 1$ the inverse function U_{sine}^{-1} maps the state variable $V_{\text{sine}} \in]-\infty, \infty[$ to the phase $\varphi \in]0, \Theta/2[$ by

$$U_{\text{sine}}^{-1}(V_{\text{sine}}) = \frac{\Theta}{\pi} \arctan\left(e^{-\frac{2\pi}{\Theta}(V_{\text{sine}} - c_1)}\right). \quad (36)$$

For the branch $k = 2$, the inverse function U_{sine}^{-1} maps the membrane potential V_{sine} in the range $] -\infty, \infty[$ to $] \Theta/2, \Theta[$,

$$U_{\text{sine}}^{-1}(V_{\text{sine}}) = -\frac{\Theta}{\pi} \arctan\left(e^{-\frac{2\pi}{\Theta}(V_{\text{sine}} - c_2)}\right) + \Theta. \quad (37)$$

Using these branches, we can now construct the transfer function $H_{\text{sine}}(\varphi)$. For this, we first consider the membrane potential dynamics and note that an input ε cannot bring V_{sine} above $+\infty$ or below $-\infty$. As a consequence, inputs do not alter the dynamical regime k . To compute the phase after an input we therefore have to use Eq. (36) if the original phase φ is within $]0, \Theta/2[$ (regime $k = 1$) and Eq. (37) if $\varphi \in]\Theta/2, \Theta[$ (regime $k = 2$). Further taking into account that the transfer function is the identity for any input at $\varphi \in \{0, \Theta/2, \Theta\}$ (the zeros of the PRC; see Sec. III A), we arrive at $H_{\text{sine}}(\varphi, \varepsilon)$:

$$H_{\text{sine}}(\varphi, \varepsilon) = \begin{cases} U_{\text{sine},1}^{-1}(U_{\text{sine}}(\varphi) + \varepsilon), & \text{for } \varphi \in]0, \frac{\Theta}{2}[, \\ U_{\text{sine},2}^{-1}(U_{\text{sine}}(\varphi) + \varepsilon), & \text{for } \varphi \in]\frac{\Theta}{2}, \Theta[, \\ \varphi, & \text{for } \varphi \in \{0, \frac{\Theta}{2}, \Theta\}, \end{cases} \quad (38)$$

$$= \begin{cases} \frac{\Theta}{\pi} \arctan\left[\tan\left(\frac{\pi}{\Theta}\varphi\right)e^{-\frac{2\pi\varepsilon}{\Theta}}\right], & \text{for } \varphi \in]0, \frac{\Theta}{2}[, \\ \frac{\Theta}{\pi} \arctan\left[\tan\left(\frac{\pi}{\Theta}\varphi\right)e^{-\frac{2\pi\varepsilon}{\Theta}}\right] + \Theta, & \text{for } \varphi \in]\frac{\Theta}{2}, \Theta[, \\ \varphi, & \text{for } \varphi \in \{0, \frac{\Theta}{2}, \Theta\}. \end{cases} \quad (39)$$

Figures 2(e) and 2(f) show the transfer function as a function of synaptic increment ε and as a function of phase φ , respectively. The panels illustrate, in particular, that φ can assume values in $[0, \Theta]$, that the neuron cannot be excited suprathresholdly, and that inputs do not give rise to transitions between the regimes $k = 1$ and $k = 2$. We note that in phase representation, we do not have to keep track of the type of the last event to execute the dynamical evolution since this information is contained in the current phase.

IV. INTERACTION SCENARIOS, ITERATION MAP, AND PHASE-LOCKING EQUATIONS

A. Interaction scenarios

In this section, we start to consider networks of two neurons, an excitatory (henceforth E) and an inhibitory (henceforth I) neuron [cf. Fig. 4(a)]. They represent two synchronized coupled neuron populations, an excitatory and an inhibitory population, by one representative neuron for each population. The couplings between the neuron populations are accounted for by couplings between the two representative neurons. We aim at setting up an event-based iteration map in the phase variables, which fully describes the network dynamics. Its fixed points and periodic orbits correspond to periodic oscillations in the phase dynamics (cf., e.g., [70]). To derive the map, we consider the difference of shifted phases of the two neurons and describe how it changes when the neurons send and receive spikes. We focus on regular periodic oscillations, where the E and I neurons spike once per cycle, argue which fixed points or periodic orbits in the dynamics correspond to ING and PING rhythms, and explore when they are generated and how they give way to each other.

We incorporate couplings from E to I (strength $\varepsilon_{E \rightarrow I}$), from I to E ($\varepsilon_{I \rightarrow E}$), and self-inhibition from I to itself ($\varepsilon_{I \rightarrow I}$). For simplicity, we do not consider self-excitation from E to itself, as it is not critically involved in PING or ING rhythms. Five events can take place in such networks: spiking of the E neuron, spiking of the I neuron, arrival of a spike from the E neuron (E spike) at the I neuron, arrival of a spike from the I neuron (I spike) at the E neuron, and arrival of an I spike at the I neuron. When an event occurs, the phase difference between the E and I neurons typically changes. We choose the conduction delay between spike sending and receiving to be τ for all connections to reduce the number of free parameters. Further, we assume that the neurons do not oscillate with too high frequencies (intrinsic period is longer than 2τ) to ensure that a spike does not arrive in the next cycle. Finally, we assume that inhibition always induces a phase delay in the E neuron. Due to the finite delay τ , spikes of the two neurons can overlap in the sense that one neuron spikes, while a spike sent by the other neuron has not yet arrived. To deal with this, we construct nonoverlapping interaction scenarios, each containing a series of events. Each of the scenarios defines a local iteration map. The local maps can be combined to a global one, G , which acts on a single variable $\Delta\psi$, the difference of shifted phases of the two neurons taking into account the differences in intrinsic period.

Without any restriction on firing activities of the E and I neurons, the events can be combinatorially combined in infinitely many ways, which results in infinitely many interaction scenarios. However, under the assumptions made in the previous paragraphs, there are five oscillation-relevant interaction scenarios; cf. the five panels in Fig. 4(b). Each interaction scenario gives rise to a local iteration map, which maps the difference of shifted phases $\Delta\psi$ before the scenario to the difference of shifted phases $\Delta\psi$ after the scenario. In scenario 1, the I neuron spikes and the spike is received before any other event, in particular, before the E neuron spikes. Similarly, in scenario 5 the E neuron spikes and the spike is received before any other event, in particular, before the I neuron spikes. In regular rhythms, scenario 1 must be followed by scenario 5 and vice versa. However, in general periodic oscillations, scenario 1 is not necessarily tied to scenario 5 and we therefore do not combine them into one scenario. We note that if scenario 1 follows shortly after scenario 5, the corresponding rhythm is PING, since the E input nearly generates the spiking of the I neuron (see Sec. VII for further discussion). If the time difference is larger, the character of the rhythm becomes unclear. However, for the considered sets of parameters around the crossing of pure ING and pure PING network oscillation frequencies, we find in our simulations that scenario 1 always follows shortly after scenario 5 in regular oscillations (less than $0.1T$, where T is the network oscillation period). For simplicity, we thus denote every scenarios 5,1 in alternation rhythm as PING in the following. We note that scenario 1 will usually not shortly precede scenario 5, since the I-spike arrival at the end of scenario 1 has a retarding effect on E-spike generation, which starts scenario 5. In scenario 2 the I neuron spikes, followed by the E neuron before the inhibitory input from the I neuron arrives and can hinder it. Since the I neuron spikes due to its own drive while the input from the E neuron arrives shortly thereafter, this scenario gives rise to

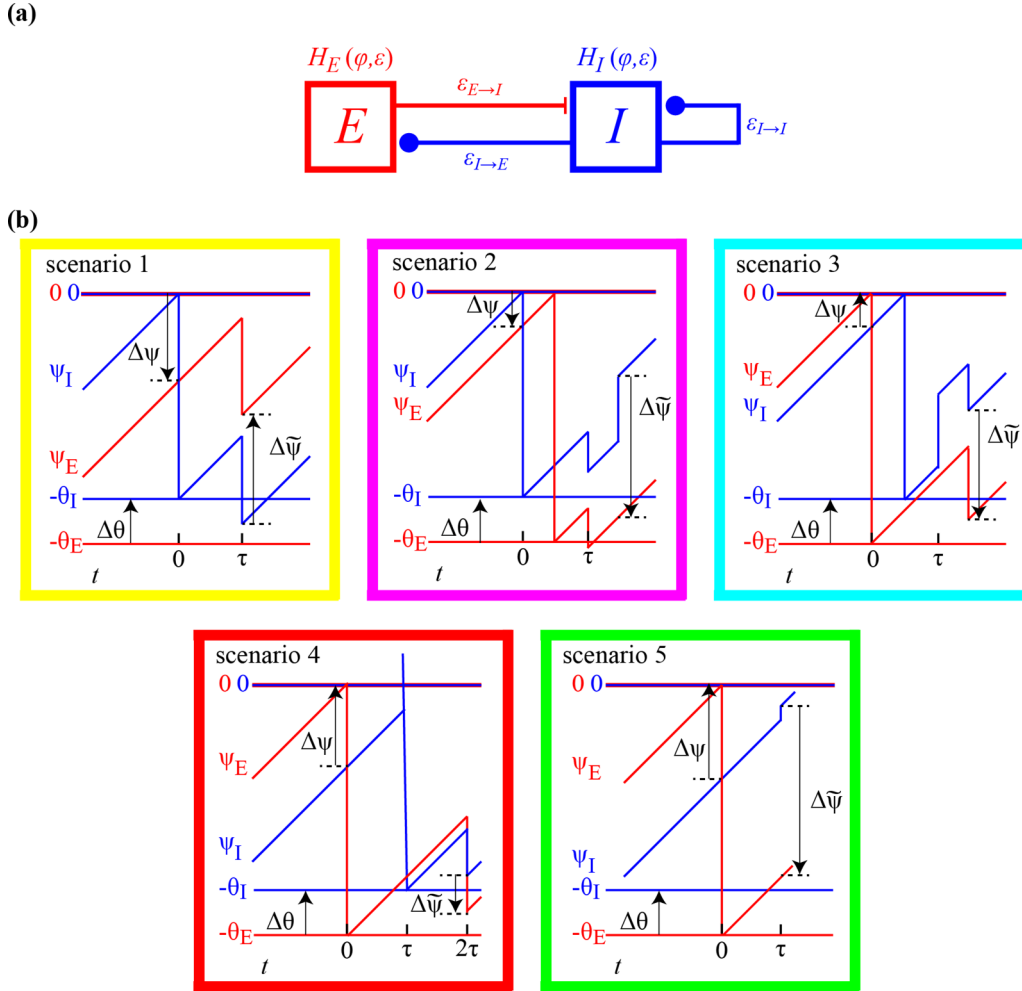


FIG. 4. Network of two neurons and illustrations of the five possible scenarios for interactions between them. Panel (a) displays the neurons (E: an excitatory neuron, I: an inhibitory neuron) and the couplings between them; their responses to inputs are governed by $H_E(\varphi, \varepsilon)$ and $H_I(\varphi, \varepsilon)$, respectively. Panels (b) show the dynamics of the shifted phases ψ_E (red) and ψ_I (blue) in scenarios 1–5. The scenarios are arranged according to the initial value of the phase difference $\Delta\psi$ [Eq. (42)], starting from large magnitude negative values.

an ING rhythm. In scenario 3, the E neuron spikes, followed by the I neuron, which spikes before the input from the E neuron arrives. Although the sequence of spiking of the E and I neurons is reminiscent of PING, this scenario also gives rise to an ING rhythm, since the I neuron does not spike due to excitatory input from the E neuron, but again due to its own drive. In scenario 4, again first the E neuron spikes, followed by the I neuron. However, the I neuron now spikes due to the excitatory input from the E neuron, which lets the I neuron exceed the spike threshold. This scenario is thus typical for PING.

B. Phase dynamics

We will now consider the interaction scenarios and their impact on the phases in detail. To identify quantities related to the E and I neurons, we endow them with an index E and I : In particular, φ_E (φ_I) and Θ_E (Θ_I) are phase and phase threshold of the E (I) neuron. To study neurons with different intrinsic periods ($\Theta_E \neq \Theta_I$), we introduce new, shifted phase variables ψ_E and ψ_I , which describe the remaining phases of the E and

I neurons to the threshold,

$$\psi_E = \varphi_E - \Theta_E, \quad (40)$$

$$\psi_I = \varphi_I - \Theta_I. \quad (41)$$

The neurons spike at $\psi_E = 0$ and $\psi_I = 0$, and the shifted phases are thereafter reset to $-\Theta_E$ and $-\Theta_I$. The remaining times to the next spiking generated by purely intrinsic dynamics are given by $-\psi_E \geq 0$ and $-\psi_I \geq 0$. We denote the differences between the new, shifted phases, the standard phases, and the phase thresholds (periods) of the neurons by

$$\Delta\psi = \psi_E - \psi_I, \quad (42)$$

$$\Delta\varphi = \varphi_E - \varphi_I, \quad (43)$$

$$\Delta\Theta = \Theta_E - \Theta_I, \quad (44)$$

respectively. Equations (40) and (41) yield the relation

$$\Delta\psi = \Delta\varphi - \Delta\Theta. \quad (45)$$

We will now derive the transition from $\Delta\psi$ before to $\Delta\tilde{\psi}$ after the sequence of interactions for scenarios 1–5 and for

a scenarios 5,1 pair. Without loss of generality, we assume $t = 0$ at the start of each scenario.

C. Scenario 1

Scenario 1, where only the I neuron spikes, occurs for

$$\Delta\psi \leq -\tau. \quad (46)$$

The phase ψ_I of the I neuron (henceforth ‘‘I phase’’) and the phase ψ_E of the E neuron (henceforth ‘‘E phase’’) at the start of the interaction sequence at $t = 0$ are

$$\psi_I = 0, \quad (47)$$

$$\psi_E = \Delta\psi. \quad (48)$$

The interaction sequence in scenario 1 consists of sending and receiving an I spike. The I neuron is reset after spiking. Thus, it receives its own spike while having the phases [cf. Eq. (1)]

$$\varphi_I(\tau) = \tau, \quad (49)$$

$$\psi_I(\tau) = \varphi_I(\tau) - \Theta_I = \tau - \Theta_I. \quad (50)$$

After input processing and thus directly at the end of the interaction sequence, the phases are

$$\tilde{\varphi}_I = H_I(\tau, \varepsilon_{I \rightarrow I}), \quad (51)$$

$$\tilde{\psi}_I = H_I(\tau, \varepsilon_{I \rightarrow I}) - \Theta_I. \quad (52)$$

The E neuron receives the I spike while having a phase $\varphi_E(0) + \tau = \Theta_E + \Delta\psi + \tau$. The phases of the E neuron directly after the interaction sequence are thus

$$\tilde{\varphi}_E = H_E(\Theta_E + \Delta\psi + \tau, \varepsilon_{I \rightarrow E}), \quad (53)$$

$$\tilde{\psi}_E = \tilde{\varphi}_E - \Theta_E = H_E(\Theta_E + \Delta\psi + \tau, \varepsilon_{I \rightarrow E}) - \Theta_E. \quad (54)$$

Equations (54) and (52) yield the phase difference after the interaction,

$$\Delta\tilde{\psi} = \underbrace{H_E(\Theta_E + \Delta\psi + \tau, \varepsilon_{I \rightarrow E}) - H_I(\tau, \varepsilon_{I \rightarrow I}) - \Delta\Theta}_{=: G(\Delta\psi)}. \quad (55)$$

G maps the difference of the shifted phases before the interaction sequence to the difference of the shifted phases thereafter.

Scenario 1 can only generate a regular oscillation (synchronization between neurons of order 1:1 [71]) together with scenario 5 (see the related paragraph below). However, scenario 1 can repeat to give rise to a regular oscillation of the I neuron, where the E neuron is suppressed. For such an oscillation, $\Delta\psi$ is given by the solution of

$$G(\Delta\psi) = \Delta\psi. \quad (56)$$

This is because $\Delta\psi$ does not change between scenarios and there is only one scenario repeating, so $\Delta\psi$ at its beginning and ending must be the same. If a real-valued solution of Eq. (56) exists, the system can generate the oscillation. Its frequency is independent of $\Delta\psi$ and may be computed as follows: The I neuron spikes at the beginning of the scenario and is reset. The generated spike arrives at the I neuron at time τ and induces an instantaneous change of the phase φ_I from τ to $H_I(\tau, \varepsilon_{I \rightarrow I})$.

To reach threshold and spike again, the I neuron needs the time $\Theta_I - H_I(\tau, \varepsilon_{I \rightarrow I})$. The period of the oscillation is the sum of the two times and the oscillation frequency is given by

$$f = [\tau + \Theta_I - H_I(\tau, \varepsilon_{I \rightarrow I})]^{-1}. \quad (57)$$

In a ‘‘pure ING’’ rhythm, the $\varepsilon_{E \rightarrow I}$ connection is deleted. While the E neuron may still spike, it does not influence the I neuron, such that its dynamics are the same as if the E neuron were suppressed. We can thus derive the oscillation frequency of the pure ING rhythm in the same manner as above and it is also given by Eq. (57).

D. Scenario 2 (a scenario leading to ING)

In scenario 2 the I neuron spikes, followed by the E neuron within time interval τ ; cf. Fig. 4(b). This happens, if before the interaction

$$-\tau < \Delta\psi < 0. \quad (58)$$

The I and E phases at the start of the interaction sequence are

$$\psi_I = 0, \quad (59)$$

$$\psi_E = \Delta\psi, \quad (60)$$

respectively. The interaction sequence consists of sending and receiving an I and an E spike. First, at $t = 0$, the I neuron sends a spike and resets, then the E neuron spikes and resets, before the I spike arrives. The reset of the I neuron implies that φ_I equals τ when it receives its own, self-inhibitory spike. Since the E spike has a conduction delay τ as well, but is sent $-\psi_E = -\Delta\psi$ after the I spike, the E spike arrives at the I neuron at $\tau - \Delta\psi$, i.e., $-\Delta\psi$ after the self-inhibitory spike. The I phase thus proceeds for $-\Delta\psi$ after the processing of the I spike before the E spike arrives. This arrival also marks the end of the interaction sequence. Taken together, the phase $\tilde{\varphi}_I$ directly after the interaction sequence (i.e., directly after receiving the E spike) reads with the interaction function H_I of the I neuron

$$\tilde{\varphi}_I = H_I(H_I(\tau, \varepsilon_{I \rightarrow I}) - \Delta\psi, \varepsilon_{E \rightarrow I}), \quad (61)$$

thus

$$\tilde{\psi}_I = \tilde{\varphi}_I - \Theta_I = H_I(H_I(\tau, \varepsilon_{I \rightarrow I}) - \Delta\psi, \varepsilon_{E \rightarrow I}) - \Theta_I. \quad (62)$$

We may assume $H_I(H_I(\tau, \varepsilon_{I \rightarrow I}) - \Delta\psi, \varepsilon_{E \rightarrow I}) < \Theta_I$; i.e., the I neuron does not spike upon arrival of the E spike, since a regular oscillation where scenario 2 begins again at its very end would require the E neuron to have an intrinsic period smaller than or equal to 2τ , which we excluded (the duration of scenario 2 is at most 2τ and the E neuron would need to reach its original phase again after its reset despite the inhibitory input). The E neuron is reset at the time $t = -\Delta\psi$ after the time of the I neuron’s spike at $t = 0$. It therefore has the phase $\tau - (-\Delta\psi) = \tau + \Delta\psi$ when the input from the I neuron arrives. The I spike changes the phase of the E neuron to $H_E(\tau + \Delta\psi, \varepsilon_{I \rightarrow E})$, where H_E is the transfer function of the E neuron. Thereafter, the E neuron evolves freely (since $\varepsilon_{E \rightarrow E} = 0$) for a time $-\Delta\psi$ until the end of the interaction sequence at

$t = (\tau - \Delta\psi)^+$. The phases then read

$$\tilde{\varphi}_E = H_E(\tau + \Delta\psi, \varepsilon_{I \rightarrow E}) - \Delta\psi, \quad (63)$$

$$\tilde{\psi}_E = \tilde{\varphi}_E - \Theta_E = H_E(\tau + \Delta\psi, \varepsilon_{I \rightarrow E}) - \Delta\psi - \Theta_E. \quad (64)$$

Taken together,

$$\Delta\tilde{\psi} = \underbrace{H_E(\tau + \Delta\psi, \varepsilon_{I \rightarrow E}) - H_I(H_I(\tau, \varepsilon_{I \rightarrow I}) - \Delta\psi, \varepsilon_{E \rightarrow I}) - \Delta\psi - \Delta\Theta}_{=:G(\Delta\psi)}. \quad (65)$$

Our considerations result again in an iteration map G , which maps the difference of the shifted phases before the interaction sequence to the difference of the shifted phases thereafter.

Scenario 2 can repeat to give rise to regular oscillations. The underlying phase dynamics then satisfy

$$G(\Delta\psi) = \Delta\psi. \quad (66)$$

Solving for $\Delta\psi$ allows us to determine the dynamics. If the E and I neurons are both LIF neurons, Eqs. (66) and (20) yield

$$\Delta\psi = \ln \left\{ \frac{e^{-\tau} - e^{-H_{\text{LIF}}(\tau, \varepsilon_{I \rightarrow I}; \Theta_I) - \Delta\Theta}}{2e^{-\Delta\Theta} \Gamma(\Theta_E, \varepsilon_{I \rightarrow E})} \pm \frac{\sqrt{[e^{-H_{\text{LIF}}(\tau, \varepsilon_{I \rightarrow I}; \Theta_I) - \Delta\Theta} - e^{-\tau}]^2 + 4e^{-\Delta\Theta} \Gamma(\Theta_E, \varepsilon_{I \rightarrow E}) \Gamma(\Theta_I, \varepsilon_{E \rightarrow I})}}{2e^{-\Delta\Theta} \Gamma(\Theta_E, \varepsilon_{I \rightarrow E})} \right\} - \Delta\Theta, \quad (67)$$

where $\Gamma(\Theta, \varepsilon)$ is defined as

$$\Gamma(\Theta, \varepsilon) := (1 - e^{-\Theta})\varepsilon. \quad (68)$$

If the I neuron is the sine neuron, Eq. (39) has to be inserted for H_I in Eq. (65). We note that the I spike arrives at the I neuron at the phase $\varphi_I = \tau$, which is in the first branch of the inverse rise function, $\varphi_I = \tau \in]0, \Theta_I/2[$, because we assume that the intrinsic period of the neuron is longer than 2τ . The input thus advances the phase and the first line of Eq. (39) will be used to write out $H_I(\tau, \varepsilon_{I \rightarrow I})$. In contrast, the E spike can arrive at a phase of the I neuron in the first branch $\varphi_I \in]0, \Theta_I/2[$ or in the second branch $\varphi_I \in]\Theta_I/2, \Theta_I[$ or at $\varphi_I = \Theta_I/2$, so it either delays or advances the phase or leaves it unchanged and the first or second or third line of Eq. (39) applies to the outer H_I in $H_I(H_I(\tau, \varepsilon_{I \rightarrow I}) - \Delta\psi, \varepsilon_{E \rightarrow I})$, depending on the value of $H_I(\tau, \varepsilon_{I \rightarrow I}) - \Delta\psi$.

If a real-valued solution $\Delta\psi$ of Eq. (66) exists, the network can generate a regular oscillation characterized by repeated occurrence of scenario 2. The oscillation frequency can be determined directly from the dynamics of the E neuron in terms of $\Delta\psi$. We start at the time when the E neuron spikes and is reset. After a time $\tau + \Delta\psi$ the inhibitory input from the I neuron arrives; cf. Eqs. (63) and (64) and the paragraph preceding them. The phase of the E neuron is changed to $H_{\text{LIF}}(\tau + \Delta\psi, \varepsilon_{I \rightarrow E}; \Theta_E)$ and it takes the E neuron the time $\Theta_E - H_{\text{LIF}}(\tau + \Delta\psi, \varepsilon_{I \rightarrow E}; \Theta_E)$ to spike again and complete the period. Summing the two times up yields the oscillation period and therewith the oscillation frequency of scenario 2 ING,

$$f(\Delta\psi) = [\tau + \Delta\psi + \Theta_E - H_{\text{LIF}}(\tau + \Delta\psi, \varepsilon_{I \rightarrow E}; \Theta_E)]^{-1}. \quad (69)$$

E. Scenario 3 (a scenario leading to ING)

In scenario 3, first the E neuron spikes and then the I neuron, before the spike from the E neuron arrives. This scenario occurs

for

$$0 \leq \Delta\psi < \tau. \quad (70)$$

The E neuron is leading, so the I and E phases at the start of the interaction sequence read

$$\psi_I = -\Delta\psi, \quad (71)$$

$$\psi_E = 0, \quad (72)$$

respectively. At time $t = 0$, the E neuron sends its spike and is reset; at time $\Delta\psi$, the I neuron sends its spike and is reset. The I neuron thus receives the E spike while having a phase $\tau - \Delta\psi$ at time τ . Processing of the E spike by the I neuron yields $H_I(\tau - \Delta\psi, \varepsilon_{E \rightarrow I})$ and subsequent time evolution until the receiving of the I spike by both the E and I neurons adds $\Delta\psi$ to the phase. We may assume $H_I(\tau - \Delta\psi, \varepsilon_{E \rightarrow I}) + \Delta\psi < \Theta_I$ and thus exclude direct generation of a spike of the I neuron because of the arrival of the spike from the E neurons, since such a spike would break a regular oscillation. Accounting for the I spike that arrives at the E and I neurons at time $\tau + \Delta\psi$, we obtain at the end of the scenario

$$\tilde{\varphi}_I = H_I(H_I(\tau - \Delta\psi, \varepsilon_{E \rightarrow I}) + \Delta\psi, \varepsilon_{I \rightarrow I}), \quad (73)$$

$$\tilde{\psi}_I = H_I(H_I(\tau - \Delta\psi, \varepsilon_{E \rightarrow I}) + \Delta\psi, \varepsilon_{I \rightarrow I}) - \Theta_I, \quad (74)$$

and

$$\tilde{\varphi}_E = H_E(\tau + \Delta\psi, \varepsilon_{I \rightarrow E}), \quad (75)$$

$$\tilde{\psi}_E = H_E(\tau + \Delta\psi, \varepsilon_{I \rightarrow E}) - \Theta_E. \quad (76)$$

We conclude

$$\Delta\tilde{\psi} = \underbrace{H_E(\tau + \Delta\psi, \varepsilon_{I \rightarrow E}) - H_I(H_I(\tau - \Delta\psi, \varepsilon_{E \rightarrow I}) + \Delta\psi, \varepsilon_{I \rightarrow I}) - \Delta\Theta}_{=:G(\Delta\psi)}. \quad (77)$$

Scenario 3 can repeat to give rise to regular oscillations. As before, if a real-valued solution of

$$G(\Delta\psi) = \Delta\psi \quad (78)$$

exists, the network can generate the oscillations and the solution $\Delta\psi$ specifies the underlying phase dynamics. The oscillation frequency can be determined directly from the dynamics of the E neuron in terms of $\Delta\psi$. At the beginning of the scenario, the E neuron spikes and at the end the E neuron's phase is given by Eq. (75). It thus spikes again after a time $\Theta_E - H_{\text{LIF}}(\tau + \Delta\psi, \varepsilon_{I \rightarrow E}; \Theta_E)$ to complete the oscillation cycle. The period of the oscillation is the sum of the duration $\tau + \Delta\psi$ of the interaction sequence and the time to complete the cycle, such that the oscillation frequency is given by

$$f(\Delta\psi) = [\tau + \Delta\psi + \Theta_E - H_{\text{LIF}}(\tau + \Delta\psi, \varepsilon_{I \rightarrow E}; \Theta_E)]^{-1}. \quad (79)$$

When the E and I neurons are LIF neurons, Eq. (78) yields

$$\Delta\psi = \ln \left\{ \frac{\Gamma(\Theta_I, \varepsilon_{I \rightarrow I}) + e^{-\tau + \Delta\Theta} - e^{-\tau}}{2\Gamma(\Theta_E, \varepsilon_{I \rightarrow E})} \pm \frac{\sqrt{[e^{-\tau} - \Gamma(\Theta_I, \varepsilon_{I \rightarrow I}) - e^{-\tau + \Delta\Theta}]^2 + 4\Gamma(\Theta_E, \varepsilon_{I \rightarrow E})\Gamma(\Theta_I, \varepsilon_{E \rightarrow I})e^{\Delta\Theta}}}{2\Gamma(\Theta_E, \varepsilon_{I \rightarrow E})} \right\} - \Delta\Theta, \quad (80)$$

where $\Gamma(\Theta, \varepsilon)$ is given by Eq. (68). Placing $\Delta\psi$ given in Eq. (80) into Eq. (79) yields the frequency of the oscillation.

If the I neuron is the sine neuron, the E spike arrives at the I neuron at a phase that is always within the first branch of the inverse rise function, i.e., within $]0, \Theta_I/2[$, because we assume that the intrinsic period of the neurons is longer than 2τ . $H_I(\tau - \Delta\psi, \varepsilon_{E \rightarrow I})$ in Eq. (77) is then explicitly defined by the first line of Eq. (39) and the excitatory input delays the phase of the I neuron. The I spike thus also always arrives at the I neuron at a phase within the first branch and advances the phase.

F. Scenario 4 (a scenario leading to PING)

In scenario 4, the E neuron spikes first, followed by the I neuron, which spikes due to suprathreshold excitatory input from the E neuron [cf. Fig. 4(b)]. We note that the scenario does not occur if the I neuron is a sine neuron because sine neurons cannot be suprathresholdly excited as the required input strength would be infinite [cf. derivation of Eqs. (38) and (39)]. In scenario 4 the E neuron spikes at $t = 0$, so the I and E phases at the start of the interaction sequence, at $t = 0$, read

$$\psi_I = -\Delta\psi, \quad (81)$$

$$\psi_E = 0, \quad (82)$$

respectively. For scenario 4, $\Delta\psi$ must satisfy

$$\tau \leq \Delta\psi \leq \Theta_I + \tau - H_I(\Theta_I, -\varepsilon_{E \rightarrow I}). \quad (83)$$

The left-hand side inequality guarantees that the I neuron does not spike before the E spike arrives. The right-hand side inequality guarantees that the I neuron is at the time of arrival of the excitatory input from the E neuron sufficiently near the threshold to receive suprathreshold excitation: The E spike arrives at time $t = \tau$ where the I neuron has phase $\psi_I = -\Delta\psi + \tau$ equivalent to $\varphi_I = \Theta_I - \Delta\psi + \tau$. The condition

that the received input is suprathreshold is then

$$U_I(\Theta_I - \Delta\psi + \tau) + \varepsilon_{E \rightarrow I} \geq U_I(\Theta_I) = \Theta_{V,I}. \quad (84)$$

We assume that $U_I(\varphi)$ is strictly monotonically increasing in the relevant range near the threshold, such that U_I^{-1} exists and is strictly monotonically increasing. We can then apply it to Eq. (84) maintaining the direction of the inequality:

$$\begin{aligned} \Theta_I - \Delta\psi + \tau &\geq U_I^{-1}(U_I(\Theta_I) - \varepsilon_{E \rightarrow I}), \\ &= H_I(\Theta_I, -\varepsilon_{E \rightarrow I}). \end{aligned} \quad (85)$$

Isolating $\Delta\psi$ yields

$$\Delta\psi \leq \Theta_I + \tau - H_I(\Theta_I, -\varepsilon_{E \rightarrow I}), \quad (86)$$

which is the right-hand side inequality of Eq. (83).

The scenario now unfolds as follows: The E neuron sends its spike and resets and the I neuron receives the E spike at $t = \tau$. The excitatory input brings the I neuron above its threshold, such that it spikes and resets subsequently. At $t = 2\tau$ both neurons receive the I spike. Due to the suprathreshold excitation the precise value of the I phase when the E spike arrives is irrelevant for the final phase. When the I neuron receives the self-inhibitory I spike at the end of the interaction sequence its phase is always $\varphi_I = \tau$, so

$$\tilde{\varphi}_I = H_I(\tau, \varepsilon_{I \rightarrow I}), \quad (87)$$

$$\tilde{\psi}_I = H_I(\tau, \varepsilon_{I \rightarrow I}) - \Theta_I. \quad (88)$$

Since the E neuron was reset at $t = 0^+$ and evolves freely until it receives the I spike at $t = 2\tau$,

$$\tilde{\varphi}_E = H_E(2\tau, \varepsilon_{I \rightarrow E}), \quad (89)$$

$$\tilde{\psi}_E = H_E(2\tau, \varepsilon_{I \rightarrow E}) - \Theta_E. \quad (90)$$

The phase difference $\Delta\tilde{\psi}$ after the interaction sequence thus reads

$$\Delta\tilde{\psi} = \underbrace{H_E(2\tau, \varepsilon_{I \rightarrow E}) - H_I(\tau, \varepsilon_{I \rightarrow I}) - \Delta\Theta}_{=:G(\Delta\psi)}. \quad (91)$$

Scenario 4 can also repeat to give rise to regular oscillations. The underlying phase dynamics then satisfy

$$G(\Delta\psi) = \Delta\psi. \quad (92)$$

Solving for $\Delta\psi$ yields

$$\Delta\psi = \ln \left[\frac{e^{-\tau} - \Gamma(\Theta_I, \varepsilon_{I \rightarrow I})}{e^{-2\tau} - \Gamma(\Theta_E, \varepsilon_{I \rightarrow E})} \right] - \Delta\Theta \quad (93)$$

(both neurons are LIF neurons for the scenario to occur). If the solution is real-valued, the network can generate the oscillation. The oscillation period can be determined directly from the dynamics of the E neuron. At the beginning of the scenario, the E neuron sends a spike and is reset. The I spike arrives after a time 2τ at the E neuron. The E phase at this point is 2τ , which changes to $H_E(2\tau, \varepsilon_{I \rightarrow E})$. The E neuron will thus spike next after a time $\Theta_E - H_E(2\tau, \varepsilon_{I \rightarrow E})$. Summing the two times up yields the oscillation period and the frequency

$$f = [2\tau + \Theta_E - H_E(2\tau, \varepsilon_{I \rightarrow E})]^{-1}. \quad (94)$$

Inserting Eq. (20) yields

$$f = \{2\tau + \Theta_E + \ln[e^{-2\tau} - \Gamma(\Theta_E, \varepsilon_{I \rightarrow E})]\}, \quad (95)$$

where Γ is defined in Eq. (68). We note that due to the suprathreshold excitation of the I neuron, the frequency is independent of $\Delta\psi$ in contrast to oscillations generated by other scenarios.

G. Scenario 5

Scenario 5 [cf. Fig. 4(b)] is similar to scenario 1, with only the E neuron spiking. It occurs for

$$\Theta_I + \tau - H_I(\Theta_I, -\varepsilon_{E \rightarrow I}) < \Delta\psi; \quad (96)$$

the phases of the I and E neurons at the start of the interaction sequence are

$$\psi_I = -\Delta\psi, \quad (97)$$

$$\psi_E = 0, \quad (98)$$

$$\Delta\tilde{\psi} = \underbrace{H_E(\Theta_I + 2\tau - H_I(\Theta_I + \tau - \Delta\psi, \varepsilon_{E \rightarrow I}), \varepsilon_{I \rightarrow E}) - H_I(\tau, \varepsilon_{I \rightarrow I}) - \Delta\Theta}_{=:G^2(\Delta\psi)}. \quad (107)$$

Note that now we have two iterations of the map G , which maps the difference of the shifted phases before scenario 5 to the difference between the shifted phases after scenario 1. To determine the phase underlying the oscillation, we need to solve

$$\Delta\psi = G^2(\Delta\psi)$$

for $\Delta\psi$. If a real-valued solution $\Delta\psi$ exists, the network can generate the oscillations. Their frequency can be derived in

respectively. The E neuron sends a spike at the beginning of the sequence, which is received by the I neuron at $t = \tau$. Since the I neuron does not spike, this marks the end of the scenario. The phase φ_I of the I neuron at receiving is

$$\varphi_I = \Theta_I - \Delta\psi + \tau. \quad (99)$$

After the receiving, at the end of the scenario the phases read

$$\tilde{\varphi}_I = H_I(\Theta_I - \Delta\psi + \tau, \varepsilon_{E \rightarrow I}), \quad (100)$$

$$\tilde{\psi}_I = H_I(\Theta_I - \Delta\psi + \tau, \varepsilon_{E \rightarrow I}) - \Theta_I. \quad (101)$$

The condition $\Theta_I + \tau - H_I(\Theta_I, -\varepsilon_{E \rightarrow I}) < \Delta\psi$ implies $H_I(\Theta_I - \Delta\psi + \tau, \varepsilon_{E \rightarrow I}) < \Theta_I$, such that the I neuron does not spike. The E neuron evolves freely after its reset at $t = 0^+$, so

$$\tilde{\varphi}_E = \tau, \quad (102)$$

$$\tilde{\psi}_E = \tau - \Theta_E, \quad (103)$$

which yields

$$\Delta\tilde{\psi} = \underbrace{\tau - H_I(\Theta_I + \tau - \Delta\psi, \varepsilon_{E \rightarrow I}) - \Delta\Theta}_{=:G(\Delta\psi)}. \quad (104)$$

H. Alternation between scenarios 5 and 1

In scenarios 2, 3, and 4 both neurons spike such that regular oscillations must be generated by repeating a single scenario. In contrast, scenarios 1 and 5 have to alternate to generate a regular oscillation. In this section, we derive the phase-locking equation and the frequency for this type of oscillation. Without loss of generality, we assume that the spiking pattern begins with scenario 5 and scenario 1 follows. $\Delta\tilde{\psi}$ at $t = 0$ has to satisfy Eq. (96) for scenario 5 to occur. $\Delta\tilde{\psi}$ after scenario 5 given in Eq. (104) has to satisfy Eq. (46) for scenario 1 to occur. Thus, alternation between scenarios 5 and 1 occurs for

$$\Theta_I + \tau - H_I(\Theta_I, -\varepsilon_{E \rightarrow I}) < \Delta\psi, \quad (105)$$

$$2\tau - \Delta\Theta \leq H_I(\Theta_I + \tau - \Delta\psi, \varepsilon_{E \rightarrow I}). \quad (106)$$

Composing the maps Eqs. (104) and (55), we obtain

terms of $\Delta\psi$: In the initial scenario 5, the E neuron spikes at time $t = 0$. The phases φ_E and φ_I at the scenario's end are given by Eqs. (100) and (102), respectively. The duration of the scenario is τ . Initializing scenario 1, the I neuron spikes after a time $\Theta_I - H_I(\Theta_I + \tau - \Delta\psi, \varepsilon_{E \rightarrow I})$. The output from the I neuron arrives at the E neuron at the phase $\varphi_E = 2\tau + \Theta_I - H_I(\Theta_I + \tau - \Delta\psi, \varepsilon_{E \rightarrow I})$ of the E neuron and causes it to jump to $H_E(2\tau + \Theta_I - H_I(\Theta_I + \tau - \Delta\psi, \varepsilon_{E \rightarrow I}), \varepsilon_{I \rightarrow E})$. The duration of scenario 1 is τ as well. The E neuron needs a time

$\Theta_E - H_E(2\tau + \Theta_I - H_I(\Theta_I + \tau - \Delta\psi, \varepsilon_{E \rightarrow I}), \varepsilon_{I \rightarrow E})$ until it spikes again and completes the oscillation cycle. The period of the spiking pattern of alternation between scenarios 5 and 1 thus equals $2\tau + \Theta_E + \Theta_I - H_I(\Theta_I + \tau - \Delta\psi, \varepsilon_{E \rightarrow I}) - H_E(2\tau + \Theta_I - H_I(\Theta_I + \tau - \Delta\psi, \varepsilon_{E \rightarrow I}), \varepsilon_{I \rightarrow E})$ and the oscillation frequency is

$$f(\Delta\psi) = [2\tau + \Theta_E + \Theta_I - H_I(\Theta_I + \tau - \Delta\psi, \varepsilon_{E \rightarrow I}) - H_E(2\tau + \Theta_I - H_I(\Theta_I + \tau - \Delta\psi, \varepsilon_{E \rightarrow I}), \varepsilon_{I \rightarrow E})]^{-1}. \quad (108)$$

V. REGULAR OSCILLATIONS

In this section we consider the regular oscillations generated by the different scenarios. In a comparably straightforward ING condition, the constant drive to the I neuron largely exceeds the constant drive to the E neuron. This gives rise to a periodic spike sequence by the I neuron, which completely inhibits spiking of the E neuron. This type of ING rhythm has been described extensively in the literature (cf., e.g., [53,54,56]). Alternatively, we can consider networks without E to I coupling; they generate the same I dynamics even if the E neuron continues to spike. Similarly well studied (cf., e.g., [54,56,72]) is the straightforward PING condition, where a relatively large drive to the E neuron causes it to spike periodically. These E spikes generate spikes in the I neuron, which has small drive and would remain rather inactive without the input from the E neuron. In this paper we will focus on situations where ING and PING are in competition since both the E and I neurons have comparably strong drives and all relevant couplings are present. However, we will consider the above-mentioned straightforward “pure ING” and “pure PING” rhythms for comparison. As described in Sec. IV, there are 5 possible scenarios for relative spiking of the E and I neurons. These can—alone or in combination—give rise to regular oscillations, more precisely to ING and PING rhythms. Scenarios 2 and 3, in which the I neuron spikes due to its intrinsic dynamics before the E input arrives, generate an ING rhythm. Scenario 4, in which the spike of the I neuron is generated by the input from the E neuron instantaneously upon its arrival, generates a PING rhythm. An oscillation generated by scenarios 5 and 1 in alternation should be interpreted as PING rhythm, if the spike of the I neuron is generated shortly after the input of the E neuron, i.e., if the input from the E neuron basically generates the I spike. If the I spike occurs with larger distance from the E spike, the character of the oscillation becomes unclear. Because for the considered parameters our simulations show spiking of the I neuron only shortly after the E input (see Sec. VII for further discussion), for simplicity we denote all scenarios 5,1 generated oscillations as PING in the following.

A. Global iteration map

The local iteration maps derived in Sec. IV are valid for $\Delta\psi$ within a certain range, where the corresponding scenario occurs. To analytically identify regular oscillations we gather the local iteration maps into a global, piecewise defined iteration map G , which maps the difference of the shifted phases $\Delta\psi$ to the difference of the shifted phases after the

next occurring interaction scenario. The global iteration map consists of several sections, since the next interaction scenario and thus the applicable map depend on the current difference of the shifted phases [e.g., Fig. 4(b)]. Equations (46), (58), (70), (83), and (96) specify the ranges, in which the different scenarios occur, and thus the domains of the individual map segments constituting G . Equations (55), (65), (77), (91), and (104) give the corresponding maps. The regular oscillations are reflected by fixed points of G (scenarios 2, 3, and 4) and G^2 (scenarios 5,1 in alternation).

B. Phased locked oscillations in networks with type I E and I neurons

Figure 5(a) shows an example of an ING rhythm (scenario 2) in a network of two type I LIF neurons in standard phase representation (cf. Sec. II). In this scenario, the I neuron (blue trace) spikes just before spiking of the E neuron (red trace) such that the inhibition from the I neuron to the E neuron arrives after spiking of the E neuron. Figure 5(c) shows the global iteration map G for the same network parameters. The panel displays the segments of the graph of G in different colors to highlight the five scenarios [see Fig. 4(b) for the color labels]. The phase differences $\Delta\psi$ that satisfy $G(\Delta\psi) = \Delta\psi$ are fixed points, which may be stable (if the absolute value of the slope of the iteration map at the fixed point is less than 1) or unstable (if the absolute value of the slope is larger than 1). The only fixed point for G in Fig. 5(c) is at the intersection of the magenta segment (scenario 2) with the diagonal (black, slope 1) near $\Delta\psi = -0.2$. It is stable. Figure 5(e) shows the iteration map after two periods, i.e., $G^2(\Delta\psi) := G(G(\Delta\psi))$. The thick segment coloring of the curve indicates the scenarios occurring in the first iteration [same as in panel (c)], while the thin curves highlight the scenarios in the second iteration. In both maps Figs. 5(c) and 5(e) the fixed point near $\Delta\psi = -0.2$ (repeated scenario 2) is the only one. It is stable and corresponds to the ING rhythm displayed in panel (a). This fixed point is robust against variations in the drive to the E and I neurons and to changes in parameter values for synaptic connectivity.

Figure 5(b) shows an example of a PING rhythm (scenario 4) in a network with two type I LIF neurons in standard phase representation. The spike from the E neuron causes excitation of the I neuron above its spiking threshold, followed by a spike and reset of the I neuron. The global iteration map G is shown in Fig. 5(d). There is a fixed point near $\Delta\psi = 0.6$ where the red segment (scenario 4) crosses the diagonal. The segment is horizontal (slope zero). This means that the fixed point is stable and that the entire range of initial phase differences $\Delta\psi$ between roughly 0.4 and 0.9 is mapped to it exactly. This can also be directly seen from Eq. (91): The right-hand side is independent of $\Delta\psi$, such that the piece of the iteration map maps any initial relative phase in its domain to the same value. The second iteration map is shown in Fig. 5(f); we find only the same fixed point as in the first iteration map.

C. Phased locked oscillations in networks with type I E and type II I neurons

As explained in Sec. IVF, networks with the type II sine I neuron cannot generate scenario 4. We therefore illustrate the

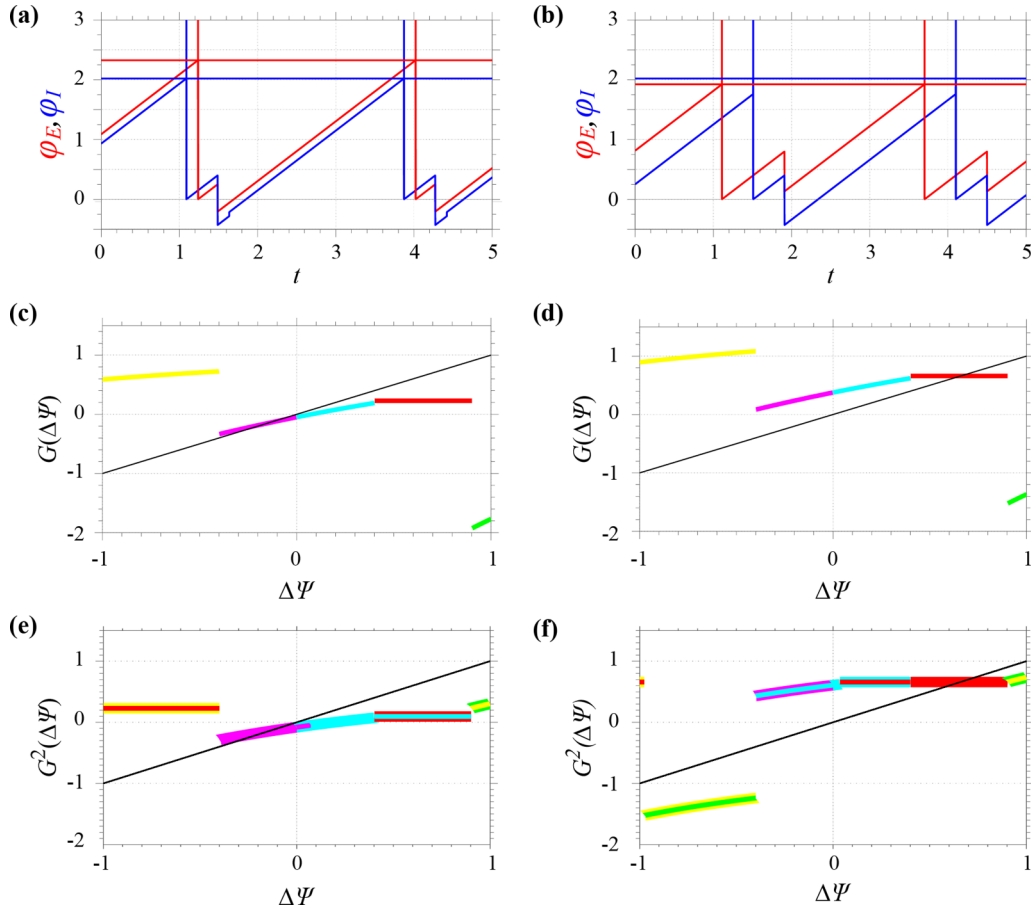


FIG. 5. ING and PING dynamics in a network of two type I (leaky integrate-and-fire) neurons. (a) ING dynamics (scenario 2) in phase representation. The panel shows φ_E (red) and φ_I (blue) versus time. Spikes are highlighted by upward vertical lines starting at the threshold. (b) PING dynamics (scenario 4) with suprathreshold excitation. (c) Iteration map G with network parameters as in (a). Pieces of the map originating from different scenarios are highlighted by different colors [scenario 1: yellow, 2: magenta, 3: cyan, 4: red, 5: green; cf. frame colors in Fig. 4(b)]. There is a stable fixed point near $\Delta\psi = -0.2$ corresponding to the ING rhythm in (a). (d) Iteration map G with network parameters as in (b). The stable fixed point near $\Delta\psi = 0.7$ corresponds to the PING rhythm in (b). Panels (e) and (f) show the second iteration maps G^2 , where the thick coloring of the segments indicates the first iteration also appearing in (c) and (d) and the thin coloring indicates the second. Parameter settings: $\varepsilon_{I \rightarrow E} = -0.5$, $\varepsilon_{E \rightarrow I} = 0.1$, $\varepsilon_{I \rightarrow I} = -1.0$, and $\tau = 0.4$; the drives to the I and E neurons are $1/\Theta_I = 0.495$ and $1/\Theta_E = 0.43$ for (a) and $1/\Theta_I = 0.495$ and $1/\Theta_E = 0.52$ for (b).

dynamics of networks with an excitatory type I LIF neuron and an inhibitory type II sine neuron with different scenarios than the dynamics of networks with two type I LIF neurons. We choose a scenario 3 ING rhythm and a scenarios 5,1 PING rhythm. We note that we observe for the considered parameters fixed points of G in the domain of scenario 2; the purple curve (scenario 2) crosses the diagonal near $\Delta\psi = -0.2$ in Fig. 6(c) and near $\Delta\psi = -0.3$ in Fig. 6(d). However, the fixed points are unstable, as the absolute value of the slope of the iteration map G is greater than 1 there. Consequently, the fixed points do not correspond to stable oscillations.

Figure 6(a) shows the ING dynamics generated by scenario 3. While the E neuron spikes just before sending of the I spike, as argued above this scenario does not belong to the class of PING, because spiking of the I neuron is not triggered by the E spike. The global iteration map G is displayed in Fig. 6(c); it has a stable fixed point near $\Delta\psi = 0.2$ in the domain of scenario 3 (intersection of the cyan curve with the diagonal). The results for the second iteration map are shown in Fig. 6(e)

with the same stable fixed point near $\Delta\psi = 0.2$ (repeated scenario 3).

Figure 6(b) shows phase dynamics that are generated by alternation of scenarios 5 and 1. We can clearly classify this pattern as PING, since excitation from the E neuron brings the I neuron close to its threshold, which results in spiking of the I neuron shortly thereafter. Figure 6(d) depicts the first iteration map G , which does not have a stable fixed point. In contrast, the second iteration map G^2 [Fig. 6(f)] has two stable fixed points, reflecting the period 2 orbit that generates the PING oscillation. They are located near $\Delta\psi = 0.6$ and $\Delta\psi = -0.7$ and correspond to alternating scenarios 5 and 1 and the phase dynamics Fig. 6(b).

VI. PING-ING INTERACTIONS IN NETWORKS OF TWO OSCILLATORS

We saw in the previous section that for suitable parameter values, our networks can generate either ING or PING rhythms.

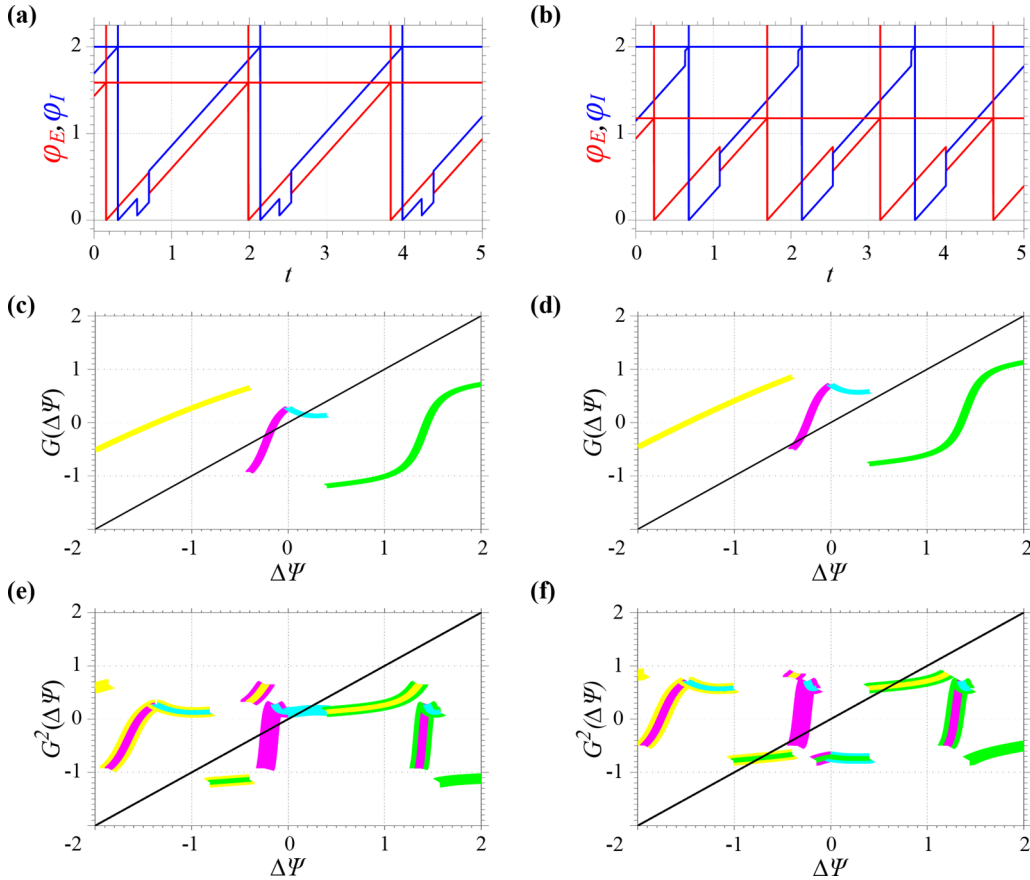


FIG. 6. ING and PING dynamics in a network of a type I (leaky integrate-and-fire) E neuron and a type II (sine) I neuron. (a) ING (scenario 3) and (b) PING (combination of scenarios 5 and 1) dynamics in phase representation. (c) and (d): Iteration maps G for the same network parameters as used in (a) and (b), respectively. The stable fixed point near $\Delta\psi = 0.2$ in (c) corresponds to the ING rhythm in (a). The other fixed point near $\Delta\psi = -0.2$ is unstable and corresponds to an unstable scenario 2 ING rhythm. (d) There is no fixed point of the first iteration map G corresponding to the PING dynamics shown in panel (b), since they consist of a sequence of two scenarios and thus appear as a period 2 orbit in the iterations of G . The unstable fixed point near $\Delta\psi = -0.3$ in (d) corresponds to an unstable scenario 2 ING rhythm. Pieces of the map generated by different scenarios are highlighted by different colors as in Fig. 5, panels (c) and (d). (e) and (f): The second iteration maps G^2 . The period 2 orbit of the PING rhythm in (b) is reflected by two fixed points in the second iteration map (f), in the domains of scenarios 1 and 5. Parameter settings: $\varepsilon_{I \rightarrow E} = -0.2$, $\varepsilon_{E \rightarrow I} = 0.5$, $\varepsilon_{I \rightarrow I} = -0.42$, and $\tau = 0.4$; the drives to the I and E neurons are $1/\Theta_I = 0.5$ and $1/\Theta_E = 0.63$ for (a) and $1/\Theta_I = 0.5$ and $1/\Theta_E = 0.85$ for (b).

In the following, we analyze how PING and ING rhythms compete to generate the network oscillation and how networks may switch from one rhythm to another when the values of the external drives change. We use “pure ING” and “pure PING” rhythms generated by reduced two-neuron networks, which do not allow for the generation of the other rhythm as reference. This allows us to better understand the competition of PING and ING rhythms in the full network, which could in principle generate both rhythms. We express the external drive given to each neuron both for the LIF and sine neuron by the inverse of the period, i.e., by $1/\Theta_E$ and $1/\Theta_I$, since—in contrast to the LIF neuron—the sine neuron does not have an explicit external driving current variable.

A. Pure PING and pure ING networks

In “pure ING” networks the only excitatory input to the I neuron is the external drive, since the synaptic strength of the projection from the E to the I neuron is set to zero (cf. also [58]). The frequency of the pure ING rhythm is determined

by the I drive and the self-inhibitory input with strength $\varepsilon_{I \rightarrow I}$ arriving a time τ after reset of the I neuron; the frequency is explicitly given by Eq. (57).

In “pure PING” networks, the I drive is sufficiently small such that the I neuron has a much lower intrinsic period than the E neuron. The circuit has a sufficiently strong projection from the E to the I neuron that each E spike brings the membrane potential of the I neuron above the threshold and elicits a spike just as in scenario 4. The frequency of the pure PING rhythm is determined by the E drive and the inhibitory input $\varepsilon_{I \rightarrow E}$ that arrives after an interval 2τ after reset of the E neuron. The frequency is explicitly given by Eq. (95).

B. Analysis of PING-ING interactions in networks with type I E and I neurons

We first study interactions between PING and ING rhythms for networks with two type I LIF neurons. The drives to the I neuron (I drive expressed by $1/\Theta_I$) and to the E neuron (E drive expressed by $1/\Theta_E$) vary; see Fig. 7. The blue surface

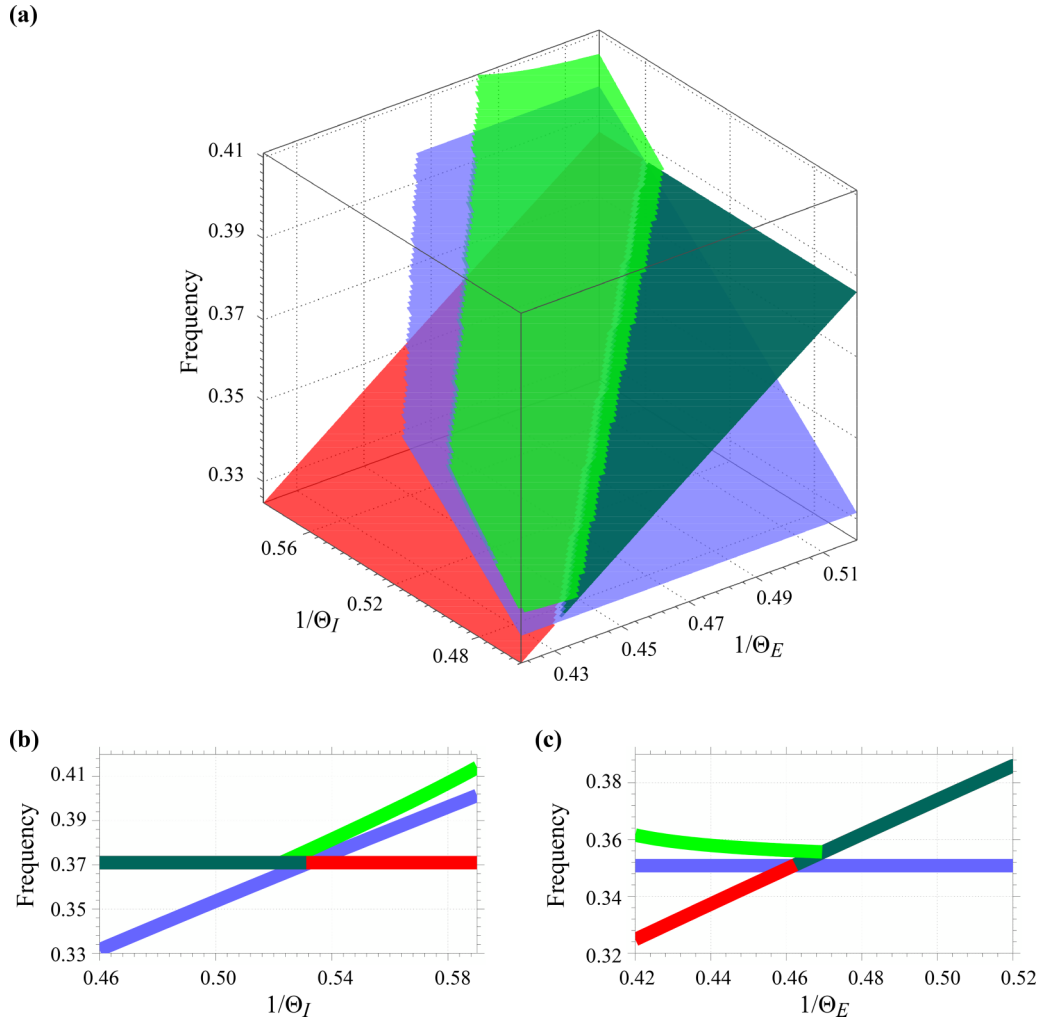


FIG. 7. Transitions between PING and ING in a network of two type I (leaky integrate-and-fire) neurons. The blue and red surfaces or curves show the oscillation frequencies of pure ING and pure PING rhythms, respectively. The green surfaces or curves show the frequency of oscillations in the full two-neuron network. Panel (a) displays the frequency of network oscillations versus the E and I drives (measured by intrinsic period⁻¹). Termination of a surface in (a) occurs at parameters $1/\Theta_E$ and $1/\Theta_I$ where the highlighted network type does not yield any regular rhythm anymore. Panels (b) and (c) show cross sections of the surfaces given in (a). The drive at the I neuron (b) or at the E neuron (c) increases from left to right while the other drive is kept fixed. Light green curves show the frequency of the full network ING rhythm while dark green curves show the frequency of the full network PING rhythm. Parameter settings: $\varepsilon_{I \rightarrow E} = -0.5$, $\varepsilon_{E \rightarrow I} = 0.1$, $\varepsilon_{I \rightarrow I} = -1.0$, and $\tau = 0.4$; in (b) the drive to the E neuron is $1/\Theta_E = 0.495$ and in (c) the drive to the I neuron is $1/\Theta_I = 0.495$.

in Fig. 7(a) shows the frequency of rhythmic spiking of the I neuron in pure ING networks. The red surface in Fig. 7(a) shows the frequency of rhythmic spiking of the E neuron in pure PING networks as a function of the E drive only. The green surface in Fig. 7(a) shows the frequency of rhythmic spiking for the full network schematically drawn in Fig. 4(a). The frequencies of the pure ING (blue surface) and of the full network (green surface) are not shown for some combinations of $1/\Theta_I$ and $1/\Theta_E$; these combinations do not elicit regular rhythms for scenarios 2, 3, and 4 and alternation of scenarios 5 and 1 for the displayed network type. Regular ING rhythms with suppressed E neuron (scenario 1 alone) are not generated either. The intersection of the surfaces in Fig. 7(a) with a plane of constant E drive ($1/\Theta_E = 0.495$) is shown in Fig. 7(b) and with a plane of constant I drive ($1/\Theta_I = 0.495$) in Fig. 7(c).

Figure 7(b) shows that for the range of comparably small I drive $1/\Theta_I$ the rhythm of the full network is PING [scenario

4; dark green line in Fig. 7(b)]. The spiking pattern of the rhythm is the same as the spiking pattern of the pure PING rhythm; cf. Fig. 5(b) for an example. The red line (pure PING) and the green line (PING for the full network) in Fig. 7(b) thus overlap. The rhythm of the full network is PING, because the E neuron recovers from the inhibition sooner than the I neuron does and the E spike elicits spiking of the I neuron at its arrival. This also implies that when the full network generates PING, its frequency is higher than the frequency of full network ING; otherwise the I neuron will spike by its own dynamics and consequently the full network generates ING. Equation (95) shows that the frequency of this PING rhythm (and the PING fixed point of the iteration map) does not depend on the I drive $1/\Theta_I$. When the I drive increases, there is a bifurcation and a (stable) scenario 3 ING solution appears near $1/\Theta_I = 0.52$ (light green curve): This ING solution lasts till near $1/\Theta_I = 0.56$, after which it switches to (stable) scenario 2

ING. The frequency of the full-network ING rhythm increases with $1/\Theta_I$. It stays higher than the frequency of pure ING because the nonzero $\varepsilon_{E \rightarrow I}$ provides an additional excitatory input to the I neuron and increases the frequency of the rhythm. Interestingly, we find coexistence of PING and ING and bistability; cf. the range $0.52 \lesssim 1/\Theta_I \lesssim 0.53$ in Fig. 7(b). As $1/\Theta_I$ increases further, the PING rhythm (dark green line) vanishes. If the network was oscillating in PING mode before, it will change to an ING rhythm and the oscillation frequency will increase in a jumplike manner.

The reason for the vanishing of the PING mode is as follows: With increasing I drive, $|\psi_I|$ (the phase distance to the threshold Θ_I) at arrival of the E spike becomes smaller until the I neuron reaches Θ_I by its intrinsic dynamics at E-spike arrival. Beyond this point, there is no PING rhythm, as the I neuron spikes before E-spike arrival. The bifurcation point is at the crossing of the pure PING line (red) and the pure ING curve (blue): Since the I neuron reaches threshold from its own drive simultaneously with the E-spike arrival, the value of $\varepsilon_{E \rightarrow I}$ becomes irrelevant. At this bifurcation point, any input will generate suprathreshold excitation and be completely canceled due to the I neuron's reset such that also the oscillation frequencies of pure PING (large $\varepsilon_{E \rightarrow I}$) and pure ING ($\varepsilon_{E \rightarrow I} = 0$) agree.

Taken together, we observe that the PING frequency is insensitive to changes in $1/\Theta_I$, while the ING frequency increases with the drive. The PING rhythm vanishes when its frequency drops below that of the pure ING rhythm and the ING rhythm vanishes when its frequency drops below that of the PING rhythm. Since the ING rhythm of the full network has higher frequency than the pure ING rhythm, we have a region of coexistence. When the full network generates ING, its frequency is always higher than the frequency of full network PING. This is due to the fact that in ING the inhibition arrives at an E phase less than 2τ and thus [Fig. 2(c)] has a smaller phase-delaying impact than in PING, where it arrives at 2τ or later. We note that the slope of the light green curve is larger than the slope of the dark green line. In other words, the ING frequency is more sensitive to a change of the I drive $1/\Theta_I$ than the insensitive PING frequency.

Figure 7(c) shows the frequency of rhythms as we fix $1/\Theta_I$ and vary $1/\Theta_E$. For small E drive [e.g., $0.42 \lesssim 1/\Theta_E \lesssim 0.46$ in Fig. 7(c)], the ING rhythm governs the dynamics of the full network: With our network parameters, it is the scenario 2 ING rhythm for $0.42 \lesssim 1/\Theta_E \lesssim 0.44$ and the scenario 3 ING rhythm for $0.44 \lesssim 1/\Theta_E \lesssim 0.46$ (present for $0.44 \lesssim 1/\Theta_E \lesssim 0.47$). As in Fig. 7(b), in Fig. 7(c) the full network ING rhythm ($\varepsilon_{E \rightarrow I} > 0$, light green) has a higher frequency than the pure ING rhythm ($\varepsilon_{E \rightarrow I} = 0$, blue line) since the nonzero excitatory input from the E neuron advances the spiking of the I neuron. The higher the E drive, the earlier does the E spike arrive in the period of the I neuron and the smaller is its excitatory effect due to the I neuron's PRC and transfer function [Fig. 2(c)]. The frequency of the ING rhythm thus slightly decreases with increasing E drive.

The absence of a PING rhythm for small E drive, where the pure ING frequency is higher than the pure PING frequency, can be understood from Eqs. (95) and (57), which specify the pure PING and pure ING frequencies, respectively. Equation (95) implies that the pure PING frequency is determined by

the interval between spikes of the E neuron, which is subject to the inhibition $\varepsilon_{I \rightarrow E}$ arriving at E phase 2τ . According to Eq. (57), the pure ING frequency is determined by the interval between spikes of the I neuron subject to the inhibition $\varepsilon_{I \rightarrow I}$. In a full network generating PING, the inhibition arrives at E phase 2τ or later, if the excitation of the I neuron is not suprathreshold. Since the delaying effect of the inhibition increases the larger the E phase is at its arrival, the spiking interval of the full network E neuron is larger or equal to that in the pure PING network. For the full network to generate PING, the spiking interval of the E neuron subject to inhibition $\varepsilon_{I \rightarrow E}$ must at least be shorter than the spiking interval of the I neuron subject to inhibition $\varepsilon_{I \rightarrow I}$ (the spiking interval in the pure ING network), since the additionally arriving excitation $\varepsilon_{E \rightarrow I}$ further decreases the spike interval of the I neuron. When already the frequency of pure ING is higher than that of pure PING, this necessary condition is violated and the PING rhythm is excluded.

As the E drive increases, the pure PING frequency starts to exceed the pure ING frequency [in Fig. 7(c) near $1/\Theta_E = 0.46$] and the full network becomes able to generate a PING rhythm. In the subsequent parameter region, the full network can generate either PING or ING depending on the initial state of the neurons. As the E drive increases further, the ING rhythm disappears [near $1/\Theta_E = 0.47$ in Fig. 7(c)]. This is because the phase advance of the I neuron due to the E spike becomes too small compared to the decreasing interval between spikes of the E neuron [Fig. 7(c): the light green curve meets the dark green one]. We note that the (negative) slope of the light green curve is smaller in absolute value than the (positive) slope of the dark green curve. In other words, the PING frequency is more sensitive to a change of the E drive $1/\Theta_E$ than the ING frequency.

C. Analysis of PING-ING interactions in networks with type I E and type II I neurons

We will now analyze interactions between PING and ING rhythms for networks with type I LIF E and type II sine I neurons for varying I and E drives; see Fig. 8. As in Fig. 7, the blue surface or curves in Fig. 8 represent the frequency of the pure ING rhythm, red stands for the pure PING rhythm, and green for full network rhythms. The frequency of the pure ING rhythm is again given by Eq. (57). The pure PING rhythm assumes spiking of the I neuron at time τ after spiking of the E neuron. The frequency of the pure PING rhythm is thus again given by Eq. (95). As mentioned above (Sec. III B), the sine I neuron without an external constant drive cannot reach the threshold for finite value of $\varepsilon_{E \rightarrow I}$; it can nevertheless get close, such that the temporal distance between E and I spike is approximately τ . We need to keep this point in mind when comparing pure PING and full network PING.

In contrast to the case of networks with type I E and I neurons, the full network with type I E and type II I neurons generates a stable oscillation with a frequency between those of pure ING and pure PING rhythms. Furthermore, our analysis reveals an unstable oscillation (scenario 2) generated by the full network, with a frequency that is much higher than the stable one for our parameters. For smaller I drive [lower $1/\Theta_I$; see Fig. 8(b)] the full network generates a PING rhythm

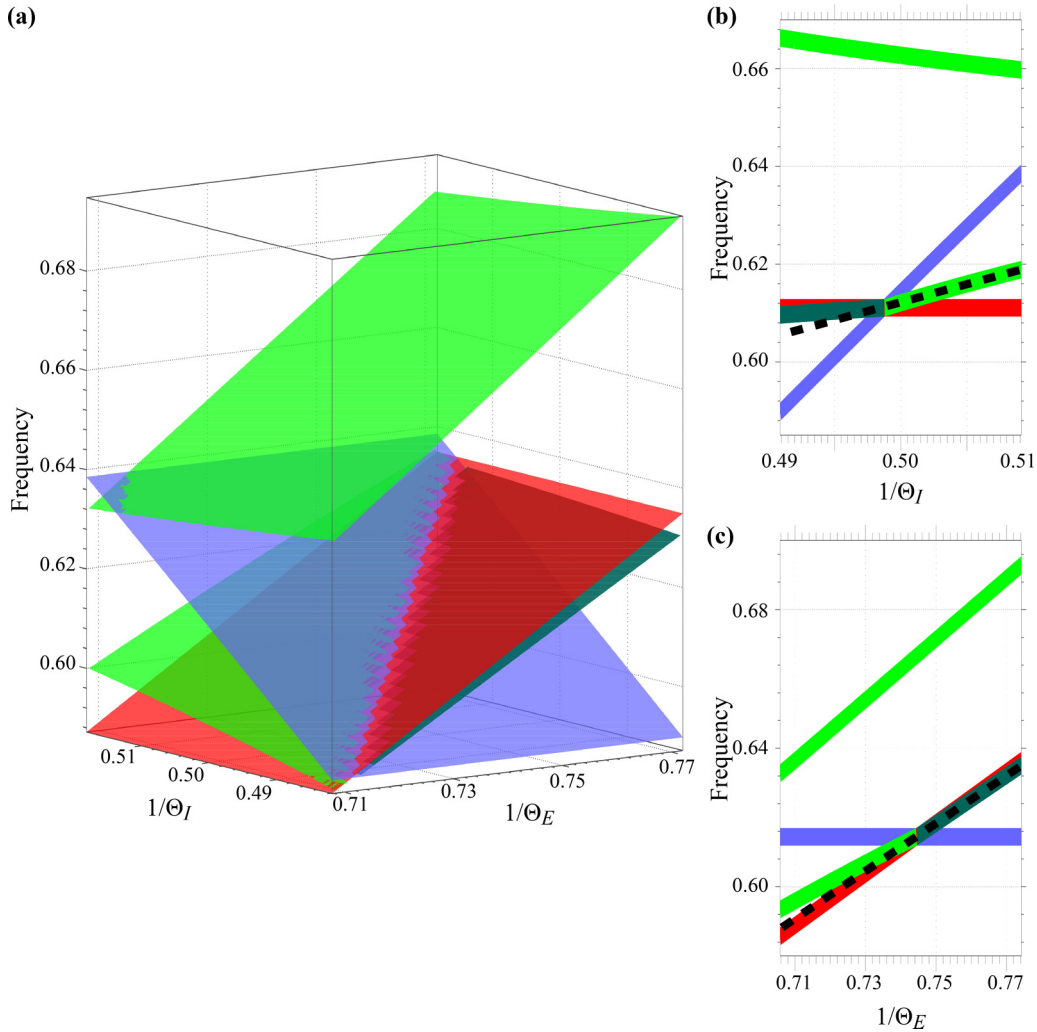


FIG. 8. Transitions between PING and ING in a network of a type I (leaky integrate-and-fire) E neuron and a type II (sine) I neuron. The blue and red surfaces or curves show the oscillation frequencies of pure ING and pure PING rhythms, respectively. The green surfaces or curves show the frequency of oscillations in the full two-neuron network. Panel (a) displays the frequency of network oscillations versus the E and I drives (measured by intrinsic period⁻¹). Panels (b) and (c) show cross sections of the surfaces given in (a): The drive of the I neuron (b) or of the E neuron (c) increases from left to right while the other drive is kept fixed. The light green (b) or the dark green (c) curves are continued by black dashed lines with the curves' average slope to allow a better comparison to the slopes of the other curves. The light green surface with comparably high frequencies in (a) and the related light green curves in (b) and (c) correspond to a scenario 2 unstable ING rhythm, while the light green surface and curves with lower frequency correspond to a scenario 3 stable ING rhythm. Dark green shows the frequency of the full network PING rhythm (scenarios 5, 1 in alternation). Parameter settings: $\varepsilon_{I \rightarrow E} = -0.2$, $\varepsilon_{E \rightarrow I} = 0.5$, $\varepsilon_{I \rightarrow I} = -0.42$, and $\tau = 0.4$; in (b) the drive to the E neuron is $1/\Theta_E = 0.74$ and in (c) the drive to the I neuron is $1/\Theta_I = 0.5$.

[alternating scenarios 5 and 1; dark green curve in Fig. 8(b)]. Its frequency is higher than the pure ING frequency; this is due to the fact that in the PING rhythm the E spike arrives in the second part of period of the sine neuron, i.e., between $[\Theta_I/2, \Theta_I]$, and it thus has an excitatory effect. Since the E spike brings the I neuron only close to its threshold Θ_I , the next spike time still depends on the I drive: The larger the drive, the shorter the time that the I neuron needs to reach the threshold after the E-spike arrival. Since this time is always at least slightly larger than zero, the full network PING frequency is lower than the pure PING frequency.

As we increase the I drive further, the full network switches from operating in PING mode to ING mode [scenario 3; light green curve in Fig. 8(b); the switch occurs near $1/\Theta_I = 0.5$].

As for networks of two type I neurons [cf. Fig. 7(b)], the rate of change of ING frequency is higher than that of PING frequency; the ING frequency is more sensitive to a change of the I drive $1/\Theta_I$ than the PING frequency [compare the dark green curve with the black dashed line in Fig. 8(b)]. The ING rhythm [light green curve in Fig. 8(b)] appears, in contrast to the case of two type I neurons, at the same point where the PING rhythm vanishes. The latter happens where the frequency of the pure ING rhythm becomes higher than that of the pure PING rhythm. This can be understood as in the case of two type I neurons, since the excitatory input in the full network PING also advances the phase of the type II I neuron. The full network ING frequency is smaller than the pure ING frequency because in the full network there is an additional input from the

E neuron. This causes a phase delay since the E spike arrives at an early phase in the spiking cycle of the type II sine neuron.

The frequency of the full network at the transition point where it switches from PING to ING is the same as the intersecting pure ING (blue curve) and pure PING (red line) frequencies. This is because at the transition point, the I neuron spikes just before the E spike arrives and the E spike meets the I neuron at a phase near zero. It therefore has a negligible effect on the phase of the sine I neuron [cf. Fig. 1(d)] and the full network behaves like the reduced ING network. Further, the I neuron's spiking and thus its effect on the E neuron is the same as in the pure PING network. So the frequencies of the full and the pure PING network are also the same.

For decreased E drive [see Fig. 8(c)], the I drive imposes an ING rhythm, which governs the dynamics of the full network, just as for networks of two type I neurons. However, as in the case of large I drive [Fig. 8(b)], for the network with the type II I neuron, we observe that the ING frequency is lower than the pure ING frequency since the E spike has a phase-delaying effect on the I neuron. The full network ING frequency is higher than the pure PING frequency since the I spike in the full network ING rhythm always arrives at an E phase less than 2τ and it thus has less inhibitory effect. When the E drive increases, there is again a transition without a coexistence region. Beyond it, the full network assumes a PING rhythm (alternation of scenarios 5 and 1). The slope of the light green curve (ING frequency) is lower than that of the dark green curve (PING frequency) [cf. light green curve and black dashed line in Fig. 8(c)]; that is, as for networks of two type I neurons, the PING frequency is more sensitive to a change of the E drive $1/\Theta_E$ than the ING frequency. Near the right-hand side of the transition point, the E spike arrives when the I neuron is near threshold. The E spike therefore brings the I neuron's phase very close to the phase threshold Θ_I , which explains why the frequency of the PING rhythm is close to the frequency of the pure PING rhythm. The PING frequency always lies below the pure PING frequency since it still takes some time for the I neuron to reach threshold after input from the E neuron. Thus, its inhibition does not arrive at the E neuron's phase 2τ but later and has a larger delaying impact.

VII. SUMMARY AND DISCUSSION

In this study, we investigate the interaction between ING and PING oscillations using an analytical approach for a simple neuronal network. In this network, two neural oscillators, an excitatory (E) and an inhibitory (I) neuron, are reciprocally connected and, additionally, the I neuron has self-inhibition. The E neuron mimics a synchronized group of pyramidal cells, while the I neuron represents a synchronized group of interneurons.

An important aspect of this model is the type of neurons (type I versus type II). Most results on the type of firing and on the PRC of pyramidal cells in the literature suggest that pyramidal cells in different brain areas belong to the category of type I neurons [73–75] (see, however, [76–78]). We adopt this view and model the E neuron as a (type I) leaky integrate-and-fire neuron. We review the derivation of the phase representation for this model, in particular, the derivation of the transfer

function H , which maps the phase of the neuronal oscillator before synaptic input to the phase after synaptic input. A full, general derivation of the phase representation for type I neurons was provided in a previous study (see [65]). The appropriate choice of interneuron phase response curve type is less clear. Oscillation-relevant interneurons can be either of type I [79] or type II [62] depending on the brain area. Therefore, we consider both options in our study: We model the I neuron as a type I leaky integrate-and-fire neuron or as a type II sine neuron. The interactions between the neurons are modeled by Dirac delta pulses, which induce a jump in the voltage of the receiving neuron by an amount that is described by the strength of the synaptic connection and independently of the voltage. In the present study we show how to derive the phase dynamics for such neural oscillators, if they have an iPRC of type II. In particular, for our type II sine I neuron, we derive the voltage dynamics and the full phase representation from its iPRC. The chosen iPRC shows a change from negative to positive as typical for type II neurons. Concretely, we use the (inverted) sine iPRC of a normal form oscillator of the Hopf bifurcation (cf. [68]). Using the phase description we can provide a full theoretical analysis of the dynamics of a network model with an E neuron and an I neuron of arbitrary type and arbitrary details of the dynamics.

Our results are also relevant for single oscillator studies, since they allow us to investigate how different an oscillator model is from a model expressible by one-dimensional voltage dynamics with voltage-independent inputs. As an example, we consider the classical radial isochron clock [1,5,80]. In this model, a point circulates on its attractor cycle in the x, y plane. Synaptic inputs cause deviations from the stable attractor cycle. Assuming that the radial deflection after an input quickly relaxes back while the change in the angular variable remains, this model reduces to a phase oscillator. For infinitesimal inputs, the resulting phase response is given by a sine iPRC. However, comparing the PRC with that in our study reveals a difference in the series expansion of the synaptic strength ε from second order on; see the Appendix.

To theoretically investigate oscillations in our two-neuron networks, we first provide a basic framework by deriving the five relevant scenarios for the change of phase differences upon interactions of the E and I neurons (see Fig. 4). This allows us to construct various modes of synchronization [71] between the two oscillators by concatenating and repeating scenarios and determining whether this results in periodic dynamics. For example, scenarios 5 and 1 can be concatenated in alternation to obtain 1:1 synchronization between the E and I oscillators. For our study, we focus on 1:1 synchronization because both the population of interneurons and the population of pyramidal cells display increased activity only once per gamma cycle [81,82].

When our two-neuron network operates in PING mode, the output of the E neuron elicits the spiking of the I neuron. This happens in scenario 4 and it can happen in the mode of alternating scenarios 5 and 1. The interpretation of a mode with repeating scenario 4 as PING is straightforward, due to the suprathreshold excitation of the I neuron. In contrast, the interpretation of modes of alternating scenarios 5,1 requires some caution. Such modes should be interpreted as PING, if the E neuron nearly excites the I neuron to spike, i.e., if

the E neuron's spike brings the I neuron so close to threshold that it spikes shortly thereafter. In the considered parameter region around the crossing of the pure PING and the pure ING network oscillation frequencies, this is the case in all our simulations of scenarios 5,1 rhythms: The I neuron spikes less than $0.1T$ after the E spike arrives, where T is the period of the rhythm. For simplicity, we therefore refer to the scenarios 5,1 rhythm as PING throughout the present article. A comparison with experimental findings corroborates our interpretation: Ref. [83] demonstrates that in PING the discharge probability of the CA3 pyramidal cells in the gamma cycle ($T \approx 18.9$ ms) reaches its maximum 3.1 ms before the maximal discharge probability of the CA3 interneurons. The latency of a monosynaptic connection is approximately 1.3 ms [84,101], so the discharge probability of the interneurons reaches a maximum 1.8 ms ($=3.1$ ms $-$ 1.3 ms) after the arrival of the inputs. This temporal difference is about $(1.8/18.9) \approx 0.1$ of the oscillation period T .

We find that when the full network operates in PING mode, its frequency is more sensitive to changes of the external drive to the E neuron than to changes of the external drive to the I neuron [see Fig. 7, panels (b) and (c), and Fig. 8, panels (b) and (c)]. When the full network operates in ING mode, the frequency more strongly depends on the external current given to the I neuron.

Our theoretical study also shows that the qualitative relation of the frequency of the full network and the frequencies of pure ING oscillations ($\varepsilon_{E \rightarrow I} = 0$) and of pure PING oscillations (no or negligible I drive) depends on whether the I neuron belongs to the category of type I or type II. When the I neuron is a type I LIF neuron, the frequency of the full network is above the pure ING and pure PING frequencies or equals the pure PING frequency. The former can be understood from the fact that the excitatory output from the E neuron to the I neuron advances the phase of the type I I neuron and therefore shortens the cycle and increases the frequency. In contrast, when the I neuron is a type II sine neuron, the frequency of the full network is between the frequencies of pure ING and pure PING. This can be understood from the fact that the excitatory input from the E neuron delays the phase of the I neuron when the spike from the E neuron arrives early in the phase of the I neuron. This increases the cycle duration and thus decreases the frequency.

Throughout the article, the type I neurons in our networks are LIF neurons. We have likewise explored networks with two type I quadratic integrate-and-fire (QIF) neurons [5] in phase representation (cf. Sec. II). In these networks with the QIF E neuron and QIF I neuron, we observe the same qualitative frequency relations as in networks of two LIF neurons, if the pure ING frequency is higher than the pure PING frequency: The frequency of the full network is slightly above the pure ING frequency. However, when the pure PING frequency is higher than the pure ING frequency, the full network frequency of coupled QIF neurons is below the pure PING frequency. This is because in the pure PING rhythm we assume that the excitatory input excites the I neuron to spike immediately at its arrival. For a QIF I neuron, this would require an infinitely large excitatory coupling strength. Since in the full network the coupling strengths are finite, the QIF I neuron cannot reach threshold instantaneously at spike arrival, in contrast to a LIF neuron. Consequently, the QIF I neuron spikes later in the

cycle and the full network frequency is lower than the pure PING frequency.

When we compare the results of the two-neuron networks, which contain two LIF or one LIF and one sine neuron, to the results from simulations in a large network of biologically more detailed pyramidal cells and interneurons, the latter show similar qualitative relations [58]: The frequency of the full network with type I interneurons is slightly above the frequency of pure ING and of pure PING, while the frequency of the full network with type II interneurons can be in between. However, the full network PING frequency of the two-neuron network with the type II I neuron is intermediate between the pure ING and pure PING frequencies [cf. Fig. 8, panels (b) and (c)], while it is slightly above for the large networks (cf. Fig. 7, panels (b) and (c), in Ref. [58]). The key to understanding this discrepancy is the net value of the excitatory output from the E neuron (or from the population of the pyramidal cells) to the I neuron (or to the population of the interneurons). In the pure PING two-neuron network the coupling is assumed to be so strong that the E spike excites the I neuron to spike immediately, while in the full two-neuron network the I neuron's phase still needs to slightly increase to reach threshold. This causes the frequency of pure PING to be higher than that of the full network. However, the net values of the excitatory outputs in both large-network topologies are approximately the same. With additional drive to the interneurons in the full large network, its frequency is thus higher than that of the pure PING large network. Another discrepancy between the results for the two-neuron network and the results for the large networks in Ref. [58] concerns network bistability. The phase iteration map of two-neuron networks with type I LIF E and I neurons has two stable fixed points (one corresponding to ING and one corresponding to PING) for parameter values near the crossing of the pure ING and pure PING frequencies, giving rise to bistability between ING and PING; see Fig. 7, panels (b) and (c). In contrast, the simulations of the large network reveal only one oscillation frequency near the crossing. Presumably, this is due to noise added to the input to the neurons in the large network. This gives rise to slightly different firing frequencies of the network's neurons, which may together obscure the bistability into a gradual transition between ING and PING. A second fixed point also occurs for the phase iteration map of the two-neuron network with the type II I neuron; cf. Figs. 6 and 8. It is unstable and corresponds to an unstable oscillation with higher frequency. In contrast, the large network simulations again reveal only one frequency. An obvious explanation is that the employed simulations cannot generate unstable oscillations due to noise. Although the results based on the two-neuron networks and the large networks [58] yield differences in some detail, the general picture is similar. In particular, the stable rhythm of the full network is usually realized by the one of ING or PING that generates the higher frequency. That is, the mechanism that generates the higher frequency "wins" in the sense that it determines the frequency of the full network. In the two-neuron network this is also the rhythm that generates the higher frequency in the corresponding pure networks. The rough explanation is that the higher frequency generating mechanism absorbs the resources necessary to maintain a rhythm: A neuron will generally spike earlier due to recruitment into a higher frequency rhythm and is

then not able to spike again to contribute to the lower frequency one. However, our analytical approaches in the present article allow for more detailed analyses; see Sec. VI.

Most studies with a large impact on the field using two-neuron (oscillator) networks were conducted either for purely inhibitory networks [85–92] or purely excitatory networks [85,90,92–96]. Studies for two-neuron networks, in which one is excitatory and another is inhibitory, are less common and many of them are in different contexts [42,74,97–99]. Börgers and Kopell [56] presented a study related to ours, but without coupling delays and assuming that $\varepsilon_{E \rightarrow I}$ is always suprathreshold. The article reports that when the intrinsic frequency of the I neuron is higher than the frequency of the PING network rhythm, the latter is destroyed via phase walk-through, which results in an irregular oscillation (the I neuron spikes more than once per cycle).

Our study considers both type I and type II I oscillators as well as a finite coupling delay. The consideration of the frequency aspect yields an intriguing dependence of the frequency changes when changing external drive, on the phase response curve of the oscillators as presented in Sec. VI.

Unlike other methods for studying the two-neuron network, our method does not focus on determining the mode of the phase locking directly but based on fundamental interaction scenarios, which can be used to construct different modes of locking under the assumption that the phase difference between the two oscillators changes only when either an input arrives or a phase is reset; the assumption is valid in our study because the connections are modeled by Dirac delta pulses. By this, we consider fast postsynaptic current (PSC) kinetics that ignores a PSC's rise and decay. Van Vreeswijk *et al.* [85] and others [100] have shown that the duration of the PSCs relative to the interval of spiking is important. Since the time constant of the synapses relevant to gamma oscillations is on the order of a few milliseconds [52,101–103], which is short against the period of gamma oscillations (around 20 ms), modeling the PSCs as delta pulses seems reasonable. The assumption that the choice of Dirac delta pulses does not affect the central conclusions of our study is also corroborated by our comparisons with biologically more detailed, larger scale networks [58].

The results of this study are relevant for *in vitro* and *in vivo* experimental studies, since they imply that a seemingly straightforward interpretation of an observed rhythm as ING or PING has to be done with care. Our findings highlight that frequent firing of the pyramidal cells does not necessarily imply that the network is dominated by PING. Similar spike patterns can be generated both by ING and by PING rhythms. In particular, the network can generate ING rhythms, where the pyramidal cells spike before the interneurons (scenario 3).

Various experiments show shifts of the frequency generated by cortical circuits when the influence of the excitatory input on the interneurons decreases due to optogenetic silencing of the local pyramidal cells *in vivo* [104] or applying an antagonist of fast excitatory synaptic coupling *in vitro* [105]. One might guess that if the cortical circuits produce oscillations whose frequency changes when one decreases the local excitatory input, the oscillations are likely to be PING because the oscillations depend on the excitation-inhibition loop. However, our studies in the two-neuron networks and in larger networks [58] suggest that knowing only that the frequency changes

when removing the local E to I inputs $\varepsilon_{E \rightarrow I}$ (by silencing pyramidal cells or disabling fast excitatory synaptic inputs) is not enough to determine whether the cortical circuits operate in either PING or ING mode. We also need to know the type of the interneurons and the direction of change of the frequency to gain information about the operation mode.

Overall, we provide a mathematical framework to construct phase oscillators that can be described by a single voltage variable with voltage-independent input, based on basically any smooth infinitesimal phase response curve. Furthermore, we construct iteration maps characterizing the dynamics of two-neuron networks. We use them to analyze how regular PING and ING oscillations in the two-neuron networks interact. Our results show that the winning mechanism (either PING or ING) is the one with the higher frequency in the full and pure networks. Except for possible small coexistence regions it will suppress the other one since it absorbs all “resources” (neurons ready to spike) available to maintain a rhythm.

ACKNOWLEDGMENTS

We thank P. Tiesinga, F. Battaglia, and S. Jahnke for fruitful discussions. The project was supported by Nederlandse Organisatie voor Wetenschappelijk Onderzoek (NWO 1105 051.02.050), by the Max Kade Foundation New York, and by Bundesministerium für Bildung und Forschung (BMBF) through the Bernstein Network (Bernstein Award 2014: 01GQ1501 and 01GQ1710).

APPENDIX: COMPARISON OF OUR SINE NEURON WITH THE RADIAL ISOCHRON CLOCK

The radial isochron clock (RIC) or Andronov-Hopf oscillator (e.g., [1,5,80]) is the normal form of oscillating systems near Hopf bifurcations. It is a two-dimensional dynamical system with the unit cycle as attractor. The dynamical equations for the radial and angular state variables are

$$\frac{dr}{dt} = \Lambda r(1 - r^2), \quad (\text{A1})$$

$$\frac{d\varphi}{dt} = 1, \quad (\text{A2})$$

with sufficiently large parameter Λ such that deflections in the radial direction are quickly eliminated and input pulses meet the system practically on the limit cycle. In contrast, angular perturbations remain; see Eq. (A2). The oscillator spikes and is reset when its angle reaches $\Theta = 2\pi$ from below. One can now posit that inputs cause a deflection into the direction of the x coordinate,

$$\begin{bmatrix} \cos(\varphi) \\ \sin(\varphi) \end{bmatrix} \rightarrow \begin{bmatrix} \cos(\varphi) + \varepsilon \\ \sin(\varphi) \end{bmatrix}; \quad (\text{A3})$$

see [5,80]. Note that by this definition an input cannot cause the oscillator to cross threshold, as it changes the state parallel to it. Assuming that we are and stay in the first quadrant, the angle changes as $\varphi \rightarrow \arctan\left(\frac{\sin(\varphi)}{\varepsilon + \cos(\varphi)}\right)$. Since the angular deflection is conserved while the radial variable relaxes to one, the phase after the input is $H_{\text{RIC}}(\varphi, \varepsilon) = \arctan\left(\frac{\sin(\varphi)}{\varepsilon + \cos(\varphi)}\right)$. If we do not stay within the first quadrant, we need to extend the

definition,

$$H_{\text{RIC}}(\varphi, \varepsilon) = \begin{cases} \arctan\left(\frac{\sin(\varphi)}{\varepsilon + \cos(\varphi)}\right), & \text{for } \varphi \in]0, \pi[\text{ and } \cos(\varphi) + \varepsilon > 0, \\ \arctan\left(\frac{\sin(\varphi)}{\varepsilon + \cos(\varphi)}\right) + \pi, & \text{for } \cos(\varphi) + \varepsilon < 0, \\ \arctan\left(\frac{\sin(\varphi)}{\varepsilon + \cos(\varphi)}\right) + 2\pi, & \text{for } \varphi \in]\pi, 2\pi[\text{ and } \cos(\varphi) + \varepsilon > 0, \end{cases} \quad (\text{A4})$$

with the appropriate continuations at the borders. The first derivative with respect to ε reads

$$\frac{\partial H_{\text{RIC}}(\varphi, \varepsilon)}{\partial \varepsilon} = -\frac{\sin(\varphi)}{1 + 2\varepsilon \cos(\varphi) + \varepsilon^2}. \quad (\text{A5})$$

Equation (A5) specifies in linear approximation the change of the current phase $H_{\text{RIC}}(\varphi, \varepsilon)$, in terms of the already received input ε and the initial phase φ . This is conceptually related to Eq. (23). It is distinct from a differential equation for the current phase, which specifies the change of the current phase in terms of the current phase [like Eq. (31)] and, if nonautonomous (see below), the independent variable, i.e., where the right-hand side would be a function of $H_{\text{RIC}}(\varphi, \varepsilon)$ and ε . For $\varepsilon = 0$ Eq. (A5) yields the iPRC. Since

$$\left. \frac{\partial H_{\text{RIC}}(\varphi, \varepsilon)}{\partial \varepsilon} \right|_{\varepsilon=0} = -\sin(\varphi), \quad (\text{A6})$$

the neuron is a sine neuron. It is, however, not the same sine neuron as ours; see Sec. III B. The transfer function of our sine neuron can be obtained via the autonomous differential equation

$$\frac{\partial H_{\text{sine}}(\varphi, \varepsilon)}{\partial \varepsilon} = Z(H_{\text{sine}}(\varphi, \varepsilon)) = -\sin[H_{\text{sine}}(\varphi, \varepsilon)], \quad (\text{A7})$$

with initial condition $H_{\text{sine}}(\varphi, 0) = \varphi$; cf. Eq. (31). The right-hand side of the equation does not depend on ε and is therefore uniquely specified by the iPRC. Solving Eq. (A7) using separation of variables yields for a neuron with period $\Theta = 2\pi$

$$H_{\text{sine}}(\varphi, \varepsilon) = \begin{cases} 2 \arctan\left[\tan\left(\frac{\varphi}{2}\right)e^{-\varepsilon}\right], & \text{for } \varphi \in]0, \pi[, \\ 2 \arctan\left[\tan\left(\frac{\varphi}{2}\right)e^{-\varepsilon}\right] + 2\pi, & \text{for } \varphi \in]\pi, 2\pi[, \end{cases} \quad (\text{A8})$$

with appropriate continuations; cf. Eq. (39). The first derivative [e.g., computed from Eq. (A7)] then explicitly reads

$$\begin{aligned} \frac{\partial H_{\text{sine}}(\varphi, \varepsilon)}{\partial \varepsilon} &= -\sin[H_{\text{sine}}(\varphi, \varepsilon)] \\ &= -\sin\left\{2 \arctan\left[\tan\left(\frac{\varphi}{2}\right)e^{-\varepsilon}\right]\right\} \\ &= -\frac{2e^\varepsilon \tan\left(\frac{\varphi}{2}\right)}{e^{2\varepsilon} + \tan\left(\frac{\varphi}{2}\right)^2}, \end{aligned} \quad (\text{A9})$$

which agrees only for $\varepsilon = 0$ with Eq. (A5). We may conclude that $H_{\text{RIC}}(\varphi, \varepsilon)$ does not obey the autonomous differential

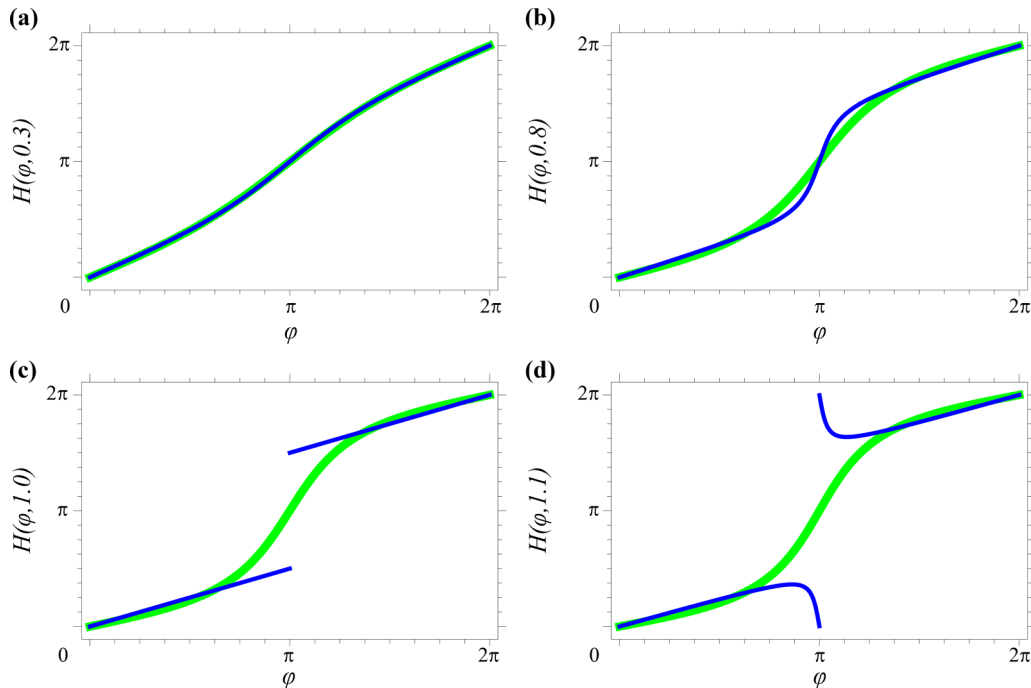


FIG. 9. Comparison of $H_{\text{sine}}(\varphi, \varepsilon)$ (green) with $H_{\text{RIC}}(\varphi, \varepsilon)$ (blue) for different values of ε . Panels (a), (b), (c), and (d) show the transfer functions for $\varepsilon = 0.3, 0.8, 1$, and 1.1 , respectively.

equation Eq. (31), but a nonautonomous one, where the right-hand side depends explicitly on the independent variable ε and which reduces to the iPRC at $\varepsilon = 0$. Graphically speaking, consider a small input piece $d\tilde{\varepsilon}$ of a total input ε . $d\tilde{\varepsilon}$ arrives after the input piece $\tilde{\varepsilon}$ of ε has already been received. Then the impact of $d\tilde{\varepsilon}$ does not only depend on the phase $\varphi(\tilde{\varepsilon}) = H_{\text{RIC}}(\varphi, \tilde{\varepsilon})$ reached due to $\tilde{\varepsilon}$ but also explicitly on $\tilde{\varepsilon}$ itself.

The series expansions in ε of $H_{\text{RIC}}(\varphi, \varepsilon)$ and $H_{\text{sine}}(\varphi, \varepsilon)$ around zero differ from second order on (they agree by definition up to first order),

$$H_{\text{RIC}}(\varphi, \varepsilon) = \varphi - \sin(\varphi)\varepsilon + \frac{1}{2} \sin(2\varphi)\varepsilon^2 - \frac{1}{3} \sin(3\varphi)\varepsilon^3 + O(\varepsilon^4), \quad (\text{A10})$$

$$H_{\text{sine}}(\varphi, \varepsilon) = \varphi - \sin(\varphi)\varepsilon + \frac{1}{4} \sin(2\varphi)\varepsilon^2 - \frac{1}{12} [\sin(3\varphi) - \sin(\varphi)]\varepsilon^3 + O(\varepsilon^4). \quad (\text{A11})$$

Equations (31) and (A7) allow us to compute expressions for the higher order derivatives and thus Taylor coefficients of its solution by differentiating both sides and replacing derivatives appearing on the right-hand side using the original equation. We note that as second derivative we obtain $\frac{\partial^2 H(\varphi, \varepsilon)}{\partial \varepsilon^2} = Z'(\varphi)Z(\varphi)$, which implies a second order Taylor coefficient $\frac{1}{2} [\sin(\varphi) \cos(\varphi)] = \frac{1}{4} \sin(2\varphi)$ as present in Eq. (A11) but not in Eq. (A10). Figure 9 illustrates the increasing discrepancy of $H_{\text{RIC}}(\varphi, \varepsilon)$ and $H_{\text{sine}}(\varphi, \varepsilon)$ for increasing ε . For $\varepsilon = 1$, $H_{\text{RIC}}(\varphi, \varepsilon)$ has a singularity (at $\varphi = \pi$) and beyond a discontinuity.

- [1] E. Izhikevich, *Dynamical Systems in Neuroscience: The Geometry of Excitability and Bursting* (MIT Press, Cambridge, 2007).
- [2] A. T. Winfree, *J. Theor. Biol.* **16**, 15 (1967).
- [3] R. M. Smeal, G. B. Ermentrout, and J. A. White, *Philos. Trans. R. Soc. London B* **365**, 2407 (2010).
- [4] R. Mirollo and S. Strogatz, *SIAM J. Appl. Math.* **50**, 1645 (1990).
- [5] P. Goel and B. Ermentrout, *Phys. D (Amsterdam, Neth.)* **163**, 191 (2002).
- [6] A. Viriyopase, I. Bojak, M. Zeitler, and S. Gielen, *Front. Comput. Neurosci.* **6**, 49 (2012).
- [7] S. Jahnke, R.-M. Memmesheimer, and M. Timme, *Phys. Rev. Lett.* **100**, 048102 (2008).
- [8] R.-M. Memmesheimer and M. Timme, *Phys. Rev. Lett.* **97**, 188101 (2006).
- [9] J. Nishimura and E. J. Friedman, *Phys. Rev. Lett.* **106**, 194101 (2011).
- [10] G. Brandner, U. Schilcher, and C. Bettstetter, *Comput. Networks* **97**, 74 (2016).
- [11] T. Forrest, J. Ariaratnam, and S. H. Strogatz, *J. Acoust. Soc. Am.* **103**, 2827 (1998).
- [12] R. Goebel, R. R. Sanfelice, and A. R. Teel, *Hybrid Dynamical Systems: Modeling, Stability, and Robustness* (Princeton University Press, Princeton, 2012).
- [13] L. Lapique, *J. Physiol. Pathol. Gén.* **9**, 620 (1907).
- [14] W. M. Kistler, W. Gerstner, and J. L. v. Hemmen, *Neural Comput.* **9**, 1015 (1997).
- [15] L. Abbott and T. B. Kepler, in *Proceedings of the XIth Sitges Conference on Statistical Mechanics of Neural Networks, Barcelona, 1990*, edited by L. Garrido (Springer-Verlag, Berlin, 1990), p. 5.
- [16] P. Dayan and L. Abbott, *Theoretical Neuroscience: Computational and Mathematical Modeling of Neural Systems* (MIT Press, Cambridge, 2001).
- [17] G. Buzsáki, *Rhythms of the Brain* (Oxford University Press, Oxford, 2006).
- [18] G. Thut, C. Miniussi, and J. Gross, *Curr. Biol.* **22**, R658 (2012).
- [19] G. Buzsáki and J. J. Chrobak, *Curr. Opin. Neurobiol.* **5**, 504 (1995).
- [20] G. Buzsáki, Z. Horváth, R. Urioste, J. Hetke, and K. Wise, *Science* **256**, 1025 (1992).
- [21] J. O'Keefe and M. L. Recce, *Hippocampus* **3**, 317 (1993).
- [22] A. Luczak, B. L. McNaughton, and K. D. Harris, *Nat. Rev. Neurosci.* **16**, 745 (2015).
- [23] E. Arabzadeh, S. Panzeri, and M. E. Diamond, *J. Neurosci.* **26**, 9216 (2006).
- [24] L. Wang, R. Narayan, G. Graña, M. Shamir, and K. Sen, *J. Neurosci.* **27**, 582 (2007).
- [25] N. Caporale and Y. Dan, *Annu. Rev. Neurosci.* **31**, 25 (2008).
- [26] R. Azouz and C. M. Gray, *Neuron* **37**, 513 (2003).
- [27] M. Volgushev, M. Chistiakova, and W. Singer, *Neuroscience* **83**, 15 (1998).
- [28] J. Jacobs, M. J. Kahana, A. D. Ekstrom, and I. Fried, *J. Neurosci.* **27**, 3839 (2007).
- [29] P. Fries, *Neuron* **88**, 220 (2015).
- [30] P. Fries, *Trends Cogn. Sci.* **9**, 474 (2005).
- [31] T. Womelsdorf, J. M. Schoffelen, R. Oostenveld, W. Singer, R. Desimone, A. K. Engel, and P. Fries, *Science* **316**, 1609 (2007).
- [32] A. M. Bastos, J. Vezoli, and P. Fries, *Curr. Opin. Neurobiol.* **31**, 173 (2015).
- [33] S. Jahnke, R.-M. Memmesheimer, and M. Timme, *Phys. Rev. E* **89**, 030701 (2014).
- [34] S. Jahnke, R.-M. Memmesheimer, and M. Timme, *PLoS Comput. Biol.* **10**, e1003940 (2014).
- [35] W. Singer, *Neuron* **24**, 49 (1999).
- [36] C. Tallon-Baudry and O. Bertrand, *Trends Cogn. Sci.* **3**, 151 (1999).
- [37] R. Eckhorn, in *The Self-Organizing Brain: From Growth Cones to Functional Networks*, Progress in Brain Research, edited by H. U. J. Van Pelt, M. A. Corner, and F. L. D. Silvar (Elsevier Science, 1994), Vol. 102, p. 405.
- [38] J. M. Palva, S. Palva, and K. Kaila, *J. Neurosci.* **25**, 3962 (2005).
- [39] W. Singer and C. M. Gray, *Annu. Rev. Neurosci.* **18**, 555 (1995).
- [40] J. E. Lisman and M. A. Idiart, *Science* **267**, 1512 (1995).
- [41] A. L. Giraud and D. Poeppel, *Nat. Neurosci.* **15**, 511 (2012).
- [42] C. Börgers and N. J. Kopell, *Neural Comput.* **20**, 383 (2008).
- [43] J. J. Hopfield, *Nature (London)* **376**, 33 (1995).
- [44] M. A. Whittington, M. O. Cunningham, F. E. LeBeau, C. Racca, and R. D. Traub, *Dev. Neurobiol.* **71**, 92 (2011).
- [45] G. Buzsáki and X. J. Wang, *Annu. Rev. Neurosci.* **35**, 203 (2012).
- [46] L. L. Colgin and E. I. Moser, *Physiology* **25**, 319 (2010).

- [47] S. R. Cobb, E. H. Buhl, K. Halasy, O. Paulsen, and P. Somogyi, *Nature (London)* **378**, 75 (1995).
- [48] W. W. Lytton and T. J. Sejnowski, *J. Neurophysiol.* **66**, 1059 (1991).
- [49] R. D. Traub, M. A. Whittington, S. B. Colling, G. Buzsáki, and J. G. Jefferys, *J. Physiol.* **493**, 471 (1996).
- [50] M. A. Whittington, R. D. Traub, and J. G. Jefferys, *Nature (London)* **373**, 612 (1995).
- [51] M. Whittington, R. Traub, N. Kopell, B. Ermentrout, and E. Buhl, *Int. J. Psychophysiol.* **38**, 315 (2000).
- [52] M. Bartos, I. Vida, and P. Jonas, *Nat. Rev. Neurosci.* **8**, 45 (2007).
- [53] N. Kopell and B. Ermentrout, *Proc. Natl. Acad. Sci. USA* **101**, 15482 (2004).
- [54] C. Börgers and N. Kopell, *Neural Comput.* **15**, 509 (2003).
- [55] P. H. Tiesinga, J. M. Fellous, J. V. José, and T. J. Sejnowski, *Hippocampus* **11**, 251 (2001).
- [56] C. Börgers and N. Kopell, *Neural Comput.* **17**, 557 (2005).
- [57] C. Börgers and B. Walker, *Front. Comput. Neurosci.* **7**, 10 (2013).
- [58] A. Viriyopase, R.-M. Memmesheimer, and S. Gielen, *J. Neurophysiol.* **116**, 232 (2016).
- [59] D. Hansel, G. Mato, and C. Meunier, *Neural Comput.* **7**, 307 (1995).
- [60] A. Erisir, D. Lau, B. Rudy, and C. S. Leonard, *J. Neurophysiol.* **82**, 2476 (1999).
- [61] T. Tateno, A. Harsch, and H. Robinson, *J. Neurophysiol.* **92**, 2283 (2004).
- [62] T. Tateno and H. Robinson, *Biophys. J.* **92**, 683 (2007).
- [63] C. van Vreeswijk, *Phys. Rev. E* **54**, 5522 (1996).
- [64] M. Timme, F. Wolf, and T. Geisel, *Chaos* **13**, 377 (2003).
- [65] R.-M. Memmesheimer and M. Timme, *Phys. D (Amsterdam, Neth.)* **224**, 182 (2006).
- [66] A. L. Hodgkin and A. F. Huxley, *J. Physiol.* **117**, 500 (1952).
- [67] B. Ermentrout, *Neural Comput.* **8**, 979 (1996).
- [68] E. N. Brown, J. Moehlis, and P. Holmes, *Neural Comput.* **16**, 673 (2004).
- [69] W. Gerstner and W. M. Kistler, *Spiking Neuron Models: Single Neurons, Populations, Plasticity* (Cambridge University Press, Cambridge, 2002).
- [70] G. B. Ermentrout and N. Kopell, *Proc. Natl. Acad. Sci. USA* **95**, 1259 (1998).
- [71] A. Pikovsky, M. Rosenblum, and J. Kurths, *Synchronization: A Universal Concept in Nonlinear Sciences* (Cambridge University Press, Cambridge, 2003).
- [72] C. Börgers, S. Epstein, and N. J. Kopell, *Proc. Natl. Acad. Sci. USA* **102**, 7002 (2005).
- [73] A. D. Reyes and E. E. Fetz, *J. Neurophysiol.* **69**, 1661 (1993).
- [74] T. I. Netoff, M. I. Banks, A. D. Dorval, C. D. Acker, J. S. Haas, N. Kopell, and J. A. White, *J. Neurophysiol.* **93**, 1197 (2005).
- [75] S. Wang, M. M. Musharoff, C. C. Canavier, and S. Gasparini, *J. Neurophysiol.* **109**, 2757 (2013).
- [76] R. F. Galán, G. B. Ermentrout, and N. N. Urban, *Phys. Rev. Lett.* **94**, 158101 (2005).
- [77] M. Lengyel, J. Kwag, O. Paulsen, and P. Dayan, *Nat. Neurosci.* **8**, 1677 (2005).
- [78] K. M. Stiefel, B. S. Gutkin, and T. J. Sejnowski, *PLoS One* **3**, e3947 (2008).
- [79] J. G. Mancilla, T. J. Lewis, D. J. Pinto, J. Rinzel, and B. W. Connors, *J. Neurosci.* **27**, 2058 (2007).
- [80] L. Glass and M. C. Mackey, *From Clocks to Chaos: The Rhythms of Life* (Princeton University Press, Princeton, 1988).
- [81] T. Gloveli, T. Dugladze, S. Saha, H. Monyer, U. Heinemann, R. D. Traub, M. A. Whittington, and E. H. Buhl, *J. Physiol.* **562**, 131 (2005).
- [82] N. Hájos, J. Pálhalmi, E. O. Mann, B. Németh, O. Paulsen, and T. F. Freund, *J. Neurosci.* **24**, 9127 (2004).
- [83] J. Csicsvari, B. Jamieson, K. D. Wise, and G. Buzsáki, *Neuron* **37**, 311 (2003).
- [84] N. Brunel and X. J. Wang, *J. Neurophysiol.* **90**, 415 (2003).
- [85] C. Van Vreeswijk, L. Abbott, and G. B. Ermentrout, *J. Comput. Neurosci.* **1**, 313 (1994).
- [86] M. Oh and V. Matveev, *J. Comput. Neurosci.* **26**, 303 (2009).
- [87] C. C. Canavier, S. Wang, and L. Chandrasekaran, *Front. Neural Circuits* **7**, 194 (2013).
- [88] A. Di Garbo, A. Panarese, M. Barbi, and S. Chillemi, *Neurocomputing* **70**, 2705 (2007).
- [89] M. Nomura and T. Aoyagi, *Prog. Theor. Phys.* **113**, 911 (2005).
- [90] B. Ermentrout, *Neural Comput.* **15**, 2483 (2003).
- [91] C. Leibold, *Phys. Rev. Lett.* **93**, 208104 (2004).
- [92] Y. D. Sato and M. Shiino, *Phys. Rev. E* **66**, 041903 (2002).
- [93] Q. Wang, Q. Lu, and G. Chen, *Int. J. Bifurcat Chaos* **18**, 1189 (2008).
- [94] U. Ernst, K. Pawelzik, and T. Geisel, *Phys. Rev. Lett.* **74**, 1570 (1995).
- [95] L. Neltner, D. Hansel, G. Mato, and C. Meunier, *Neural Comput.* **12**, 1607 (2000).
- [96] M. Dhamala, V. K. Jirsa, and M. Ding, *Phys. Rev. Lett.* **92**, 074104 (2004).
- [97] S. R. Jones, D. J. Pinto, T. J. Kaper, and N. Kopell, *J. Comput. Neurosci.* **9**, 271 (2000).
- [98] M. A. Kramer, A. K. Roopun, L. M. Carracedo, R. D. Traub, M. A. Whittington, and N. J. Kopell, *PLoS Comput. Biol.* **4**, e1000169 (2008).
- [99] S. Lee, K. Sen, and N. Kopell, *PLoS Comput. Biol.* **5**, e1000602 (2009).
- [100] S. Jahnke, R.-M. Memmesheimer, and M. Timme, *Front. Comput. Neurosci.* **3**, 13 (2009).
- [101] J. R. Geiger, J. Lübke, A. Roth, M. Frotscher, and P. Jonas, *Neuron* **18**, 1009 (1997).
- [102] M. Bartos, I. Vida, M. Frotscher, A. Meyer, H. Monyer, J. R. Geiger, and P. Jonas, *Proc. Natl. Acad. Sci. USA* **99**, 13222 (2002).
- [103] M. C. Angulo, J. Rossier, and E. Audinat, *J. Neurophysiol.* **82**, 1295 (1999).
- [104] M. T. Craig and C. J. McBain, *J. Neurosci.* **35**, 3616 (2015).
- [105] F. E. N. LeBeau, S. K. Towers, R. D. Traub, M. A. Whittington, and E. H. Buhl, *J. Physiol.* **542**, 167 (2002).